Constitutive framework for rheologically complex interfaces with an application to elastoviscoplasticity

Journal of Non-Newtonian Fluid Mechanics 301 (2022) 104726

Contents lists available at ScienceDirect

Journal of Non-Newtonian Fluid Mechanics

journal homepage: www.elsevier.com/locate/jnnfm

Constitutive framework for rheologically complex interfaces with an application to elastoviscoplasticity

M.A. Carrozza, M. Hütter *, M.A. Hulsen, P.D. Anderson

Polymer Technology, Department of Mechanical Engineering, Eindhoven University of Technology, PO Box 513, 5600 MB Eindhoven, The Netherlands

ARTICLE INFO

Keywords:
Interfacial rheology
Constitutive modelling
Elastoviscoplasticity
Yield stress materials
Non-linear viscoelasticity
Numerical calculations

ABSTRACT

A framework is presented for the formulation of a class of continuum constitutive models for sharp interfaces with non-linear viscoelastic behaviour due to a considerable isotropic interfacial microstructure. For the formulation of a thermodynamically consistent elastoviscoplastic interface constitutive model we adapt an approach successful in describing the behaviour of bulk polymer glasses. The model has a clear separation between dilatation and shear, and is used to predict phenomena related to the plasticity of interfaces observed in the experimental literature, which is relevant for many applications. Stress–strain predictions in standard interfacial rheological flows, i.e. shear and dilatation, are investigated numerically. A predominantly elastic response is obtained at small deformations, with a transition to primarily plastic flow at high stress levels. In interfacial shear flow, strain softening and eventually a plastic plateau occur upon further deformation beyond the yield point. The yield stress and strain and (the relative strength of) the stress overshoot in interfacial shear flow are shown to be controlled by two dimensionless groups of parameters in the model. In interfacial dilatation, the model predicts elastoviscoplastic behaviour with a stress maximum and a decreasing stress without a plateau at even larger deformations. These phenomena are studied for various choices for the parameters in the model.

1. Introduction

Plastic behaviour of fluid–fluid interfaces in foams and emulsions is relevant in many applications such as foods, consumer products, pharmaceuticals (drug delivery), petrochemicals (oil recovery), polymer technology (polymer blends), and also in nature and biology. The larger the ratio between interfacial surface area and bulk fluid volume, or the smaller the corresponding length scale, the more the interfacial properties affect the overall mechanical behaviour of foams and emulsions. An example of the effectiveness of interfacial plasticity is the stability of foams and emulsions, where the strength of the interface should be high enough to prevent bubble or drop coalescence upon collision. Yield-stress interfaces contribute for a large part to other macroscopic material properties, e.g. to the bulk yield stress of foams/emulsions [1]. The single and collective behaviour of bubbles/drops where interfacial yielding plays a role includes e.g. the deformation, break-up, coalescence, collision or closely approaching/passing of drops/bubbles, and film drainage between drops/bubbles. These phenomena are all relevant for applications and require further investigation.

Experimental results on interfacial plasticity (measurements and observations) have been reported extensively in the literature for all kinds of different interfacial microstructures, e.g. particles, proteins, lipids, (bio)polymers, asphaltenes, surfactant molecules. The experiments use interfacial shear and dilatational/extensional rheometers with well-defined kinematics, see for example [2–10]. The mechanical behaviour of these systems is characterised by the presence of an interfacial yield stress/strain with a transition from predominantly elastic solid behaviour to primarily plastic flow, i.e. elastoviscoplastic behaviour. For example, a strain-amplitude sweep in interfacial large-amplitude oscillatory shear (LAOS) experiments has been performed by Zang et al. [2]. Similar to strain sweeps in interfacial LAOS, Jung et al. [3] performed step interfacial shear rate experiments in which the interfacial shear stress is measured as a function of interfacial shear strain, but here a constant interfacial shear rate is imposed. In these experiments, although for different interfacial microstructures, i.e. different surfactant types, qualitatively similar behaviour was observed. A linear dependence of the interfacial shear stress was measured at smaller interfacial shear strains, followed by a stress maximum, the interfacial yield stress, at the yield strain. Subsequently, the stress decreases with increasing strain and eventually finds a plateau value. The results from Martin et al. [4] for step interfacial shear rate also

* Corresponding author.
E-mail addresses: m.a.carrozza@tue.nl (M.A. Carrozza), m.huetter@tue.nl (M. Hütter), m.a.hulsen@tue.nl (M.A. Hulsen), p.d.anderson@tue.nl (P.D. Anderson).

https://doi.org/10.1016/j.jnnfm.2021.104726
Received 29 July 2021; Received in revised form 10 December 2021; Accepted 11 December 2021
Available online 5 January 2022

show this linear increase of the shear stress for smaller shear strains. However, their results do not show a decrease in the shear stress beyond the yield point followed by a plateau. Instead, either a yield-stress plateau is attained immediately, or a continuing stress increase with a constant but much smaller slope than in the linear regime. In interfacial large amplitude oscillatory extension and step extensional strain (rate) experiments, similar results as for their interfacial shear experiment counterparts have been obtained [5–7]. Note, that these experiments include pure dilatation, which is applying an isotropic extensional strain, and uniaxial extension, by which we mean imposing an extensional strain in one direction of the interface while keeping the strain in the other direction fixed. In contrast to shear experiments, for extension in [5–7] no overshoot in the stress was observed during plastic flow.

When it comes to modelling the non-linear viscoelasticity of interfaces, two approaches are followed in the literature. A first is straightforward generalisation of bulk constitutive models [11], such as the Boussinesq–Scriven viscous compressible interface model [12] and the Hütter–Tervoort hyperelastic compressible interface model [13,14]. The other approach is using thermodynamic formalisms for multiphase systems to construct admissible interface constitutive models, consistent with the second law of thermodynamics [13,15]. A linear Maxwell constitutive equation for interfaces is obtained by writing down an expression for the interfacial entropy-production rate and constructing a differential constitutive equation for the interfacial stress tensor by linear expansion [15]. To obtain a frame-invariant non-linear viscoelastic interface model without loss of generality, the surface material derivative in the equation for the deviatoric stress is replaced by the surface upper-convected derivative, yielding the surface upper-convected Maxwell model [11]. In a similar fashion, other thermodynamically admissible non-linear viscoelastic models can be constructed, such as the interfacial Giesekus model [15].

In this paper, we introduce a continuum modelling framework for describing non-linear viscoelastic behaviour of sharp interfaces. An adequate approach for modelling the elastoviscoplasticity of bulk polymer glasses is adapted to describe the kinematics and stress of isotropic interfaces with behaviour in between that of a fluid and a solid. We use a Lagrangian description of the interface and assume that there is no mass transport across the interface. Our aim is to develop a rheologically complex interface modelling framework that can be implemented in numerical multiphase flow solvers, as described in e.g. [11,16–20]. The kinematics for describing arbitrary large deformations and the deformation rate of differentiable interfaces are explained in Section 2. Section 3 provides general expressions for thermodynamically admissible constitutive relations for the plastic surface rate-of-deformation tensor and the interfacial stress tensor. Interface versions of well-known viscoelastic bulk fluid models are presented in the rest of Section 3, whereas Section 4 introduces our elastoviscoplastic interface model. Model predictions of the elastoviscoplastic interface model for interfacial simple shear and dilatational flow, obtained by numerical calculations, are shown in Section 5. These results demonstrate that for these simple flows we can qualitatively describe the elastoviscoplastic behaviour of interfaces observed in the literature. In Section 6, the model is discussed in comparison with its counterpart for bulk materials. Conclusions are drawn and recommendations for further research are given in Section 7.

2. Kinematics of interfaces

We start in Section 2.1 with a recap and discussion on curvilinear surface coordinates and how to write interfacial tensors, vectors and derivative operators in such a coordinate system, since this will be used throughout the paper. Interfacial tensors, vectors and derivative operators appearing in this paper are defined on the interface only, i.e. they are functions of position within the interface only, and are denoted by a subscript $()_s$. For interfacial vectors and operators this subscript means that these are directed tangential to the interface. However, they are still described as vectors in 3D space. On the contrary, tensors with this subscript are not necessarily directed tangential to the interface and can have additional out-of-plane directions that are perpendicular to the interface. However, at least the left-hand or the right-hand side of the tensor has directions that are tangential to the interface, unless otherwise stated. All interfacial tensors in this paper are 3D tensors of rank two, which means that one of the eigenvalues equals zero. Which of the two sides of the interfacial tensors has out-of-plane directions will be clarified for each tensor where it is introduced, and a separate table will be presented that summarises this, see Table A.1.

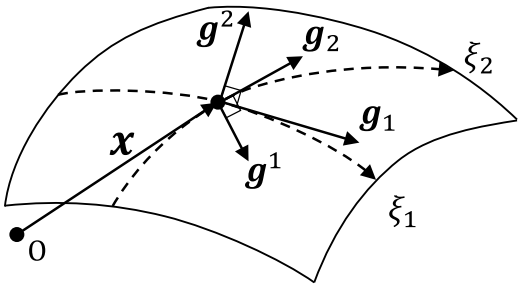

Fig. 1. Schematic representation of a cut-out of the interface on which points with 3D spatial position $\boldsymbol{x}$ are described by curvilinear coordinates $\underset{\sim}{\xi} = (\xi_1, \xi_2)$. Also depicted are covariant base vectors $\boldsymbol{g}_i$ and contravariant base vectors $\boldsymbol{g}^i$.

The kinematics for describing arbitrarily large deformations of interfaces are explained in Section 2.2 and from this, the rate of deformation of interfaces is derived in Section 2.3. We follow a Lagrangian approach and assume no transfer of mass across the interface. Einstein summation convention is used in the following, where summation is performed over repeated indices in the same term of an equation. In the literature, the adjectives 'surface' and 'interfacial' are used interchangeably to introduce tensors, vectors and derivative operators defined on the interface. We will also use this nomenclature.

2.1. Curvilinear coordinates

For a mathematical description of the deformation and rheological behaviour of differentiable interfaces, it is convenient to use curvilinear surface coordinates. All the quantities related to the interface only live within and vary along the interface, which has a curved geometry in general. These curvilinear coordinates are used to define local vector bases that are tangential to the interface, with respect to which interfacial vectors, tensors and derivative operators can then be described. For this purpose, the interface position $\boldsymbol{x}$ in 3D space is parametrised according to

$$\boldsymbol{x} = \boldsymbol{\mathcal{X}}(\underset{\sim}{\xi}, t), \tag{1}$$

where $\boldsymbol{\mathcal{X}}$ is the function that uniquely maps the curvilinear surface coordinates $\underset{\sim}{\xi} = (\xi_1, \xi_2)$ onto the position $\boldsymbol{x}$ of the corresponding point on the surface in 3D space, see Fig. 1. The base vectors $\boldsymbol{g}_i$, $i = 1, 2$, also called covariant base vectors, are given by

$$\boldsymbol{g}_i = \frac{\partial \boldsymbol{x}}{\partial \xi_i}, \qquad i = 1, 2, \tag{2}$$

with the index i running from 1 to 2 since the interface is two-dimensional. A dual basis is introduced by defining the biorthogonal system

$$\boldsymbol{g}_i \cdot \boldsymbol{g}^j = \begin{cases} 1, & i = j \\ 0, & i \neq j \end{cases} \equiv \delta_{ij}, \qquad i, j = 1, 2, \tag{3}$$

where $\boldsymbol{g}^j$, $j = 1, 2$, are the dual or contravariant base vectors, and δ_{ij} is the Kronecker delta. In the following, we will omit $i, j = 1, 2$. Note that, in general $\boldsymbol{g}_i$ are neither necessarily mutually perpendicular nor

of unit length and the same also holds for $\boldsymbol{g}^i$. However, all four vectors must be tangential to the interface. The vectors $\boldsymbol{g}_i$ and $\boldsymbol{g}^i$ can also be expressed in terms of each other:

$$\boldsymbol{g}_i = g_{ij}\boldsymbol{g}^j, \tag{4}$$

$$\boldsymbol{g}^i = g^{ij}\boldsymbol{g}_j, \tag{5}$$

with the (covariant) metric matrix g_{ij} and dual (or contravariant) metric matrix g^{ij} given by

$$g_{ij} = \boldsymbol{g}_i \cdot \boldsymbol{g}_j, \tag{6}$$

$$g^{ij} = \boldsymbol{g}^i \cdot \boldsymbol{g}^j. \tag{7}$$

Eqs. (4)–(5) give the rules for moving indices "up and down". The metric matrices are symmetric and are each other's inverse:

$$g^{ij} = g_{ij}^{-1}, \qquad \text{or} \qquad g^{ik}g_{kj} = \delta_{ij}, \tag{8}$$

which can be seen by premultiplying Eq. (4) by g_{ki}^{-1} and then comparing with Eq. (5).

Using curvilinear surface coordinates, arbitrary interfacial vectors $\boldsymbol{v}_\mathrm{s}$ and tensors $\boldsymbol{T}_\mathrm{s}$, of which the directions are only tangential to the interface, such as the interfacial stress tensor $\boldsymbol{\tau}_\mathrm{s}$, can now also be expressed in terms of covariant base vectors $\boldsymbol{g}_i$ and contravariant base vectors $\boldsymbol{g}^i$. Using Eq. (3) these can be written as

$$\boldsymbol{v}_\mathrm{s} = v_\mathrm{s}^i\boldsymbol{g}_i = v_{\mathrm{s},i}\boldsymbol{g}^i, \tag{9}$$

$$\boldsymbol{T}_\mathrm{s} = T_\mathrm{s}^{ij}\boldsymbol{g}_i\boldsymbol{g}_j = T_{\mathrm{s},ij}\boldsymbol{g}^i\boldsymbol{g}^j, \tag{10}$$

with contravariant components $v_\mathrm{s}^i = \boldsymbol{v}_\mathrm{s}\cdot\boldsymbol{g}^i$ and $T_\mathrm{s}^{ij} = \boldsymbol{g}^i\cdot\boldsymbol{T}_\mathrm{s}\cdot\boldsymbol{g}^j$, and covariant components $v_{\mathrm{s},i} = \boldsymbol{v}_\mathrm{s}\cdot\boldsymbol{g}_i$ and $T_{\mathrm{s},ij} = \boldsymbol{g}_i\cdot\boldsymbol{T}_\mathrm{s}\cdot\boldsymbol{g}_j$. Note that the rules for moving indices up and down, given by Eqs. (4)–(5), are also valid for the components, e.g. $v_\mathrm{s}^i = g^{ij}v_{\mathrm{s},j}$.

The surface unit tensor $\boldsymbol{I}_\mathrm{s} = \boldsymbol{I} - \boldsymbol{nn}$, with $\boldsymbol{n}$ the unit-normal vector on the interface, can be written in the four equivalent representations

$$\boldsymbol{I}_\mathrm{s} = \boldsymbol{g}_i\boldsymbol{g}^i = \boldsymbol{g}^i\boldsymbol{g}_i = g^{ij}\boldsymbol{g}_i\boldsymbol{g}_j = g_{ij}\boldsymbol{g}^i\boldsymbol{g}^j, \tag{11}$$

where the first two follow from substituting $v_\mathrm{s}^i = \boldsymbol{v}_\mathrm{s}\cdot\boldsymbol{g}^i$ and $v_{\mathrm{s},i} = \boldsymbol{v}_\mathrm{s}\cdot\boldsymbol{g}_i$ into Eq. (9) and then requiring that Eq. (9) must hold for all $\boldsymbol{v}_\mathrm{s}$. The last two representations in Eq. (11) are obtained by substituting Eqs. (4)–(5) into the first two steps. The expressions for $\boldsymbol{I}_\mathrm{s}$ in Eq. (11) are equivalent, but we will prefer one over the other depending on the context. Note that $\boldsymbol{I}_\mathrm{s}$ is in general a function of position on the interface and of time, contrary to the rank-3 unit tensor.

The surface gradient operator, the gradient operator along the interface, is defined as

$$\boldsymbol{\nabla}_\mathrm{s} = \boldsymbol{g}^i\frac{\partial}{\partial\xi_i}. \tag{12}$$

The direction of $\boldsymbol{\nabla}_\mathrm{s}$ is tangential to the interface since $\boldsymbol{g}^i$ are tangential vectors. Also, $\boldsymbol{\nabla}_\mathrm{s}\boldsymbol{x} = \boldsymbol{g}^i\partial\boldsymbol{x}/\partial\xi_i = \boldsymbol{g}^i\boldsymbol{g}_i = \boldsymbol{I}_\mathrm{s}$, where Eqs. (2), (11) and (12) have been used.

2.2. Deformation

2.2.1. Surface deformation tensors

To derive models that are valid for arbitrarily large deformations written in terms of finite strain tensors, we make use of the surface deformation gradient tensor $\boldsymbol{F}_\mathrm{s}$ to describe the deformation. The tensor $\boldsymbol{F}_\mathrm{s}$ maps an infinitesimal material line element $d\boldsymbol{x}_0$ between two particles on the interface in the reference configuration onto an infinitesimal material line element $d\boldsymbol{x}$ between the same two particles on the deformed interface in the current configuration. In the following, we will use the subscript $()_0$ if the corresponding quantity or derivative operator is evaluated at the reference time t_0, e.g. $\boldsymbol{g}_{i,0} = \boldsymbol{g}_i(t = t_0)$. Since we only consider a Lagrangian description in this paper, the curvilinear coordinates $\underset{\sim}{\xi}$ can be used as interface material point labels. Hence, we can determine the interface position $\boldsymbol{x}_0$ in a reference configuration at time t_0 using Eq. (1) as

$$\boldsymbol{x}_0 = \boldsymbol{\mathcal{X}}(\underset{\sim}{\xi}, t = t_0). \tag{13}$$

The surface deformation gradient tensor $\boldsymbol{F}_\mathrm{s}$ is defined by (see [21])

$$d\boldsymbol{x} = \boldsymbol{F}_\mathrm{s}\cdot d\boldsymbol{x}_0, \tag{14}$$

and can be expressed as

$$\boldsymbol{F}_\mathrm{s} = \boldsymbol{g}_i\boldsymbol{g}_0^i = (\boldsymbol{\nabla}_{\mathrm{s},0}\boldsymbol{x})^\mathrm{T}, \tag{15}$$

which can be shown by substituting $d\boldsymbol{x} = \boldsymbol{g}_i d\xi_i$ into Eq. (14) and using Eqs. (2), (3) and (12). Note that the directions of $\boldsymbol{F}_\mathrm{s}$ on its left-hand side are tangential to the interface in the current configuration, whereas on its right-hand side the directions are tangential to the interface in the reference configuration. In case of no deformation, the reference and current configurations are the same, and thus $\boldsymbol{F}_\mathrm{s}(t = t_0) = \boldsymbol{I}_{\mathrm{s},0}$ (see Eqs. (11) and (15)).

The relative change in interfacial surface area J_s is defined as the ratio between a surface area element dA spanned by two infinitesimal interface material line elements in the current configuration $d\boldsymbol{x}_1$ and $d\boldsymbol{x}_2$, and the surface area element dA_0 spanned by two infinitesimal interface material line elements in the reference configuration $d\boldsymbol{x}_{0,1}$ and $d\boldsymbol{x}_{0,2}$. Using the covariant base vectors, it is expressed as

$$J_\mathrm{s} = \frac{dA}{dA_0} = \frac{\|\boldsymbol{g}_1\times\boldsymbol{g}_2\|}{\|\boldsymbol{g}_{1,0}\times\boldsymbol{g}_{2,0}\|} \equiv \det_\mathrm{s}(\boldsymbol{F}_\mathrm{s}), \tag{16}$$

where $\det_\mathrm{s}$ is the surface determinant [21].

The Moore–Penrose inverse [22,23], a generalisation of the inverse tensor applied to rank-2 tensors in this paper, of $\boldsymbol{F}_\mathrm{s}$, is defined by $d\boldsymbol{x}_0 = \boldsymbol{F}_\mathrm{s}^{-1}\cdot d\boldsymbol{x}$ (see Eq. (14)), and can be expressed as

$$\boldsymbol{F}_\mathrm{s}^{-1} = \boldsymbol{g}_{j,0}\boldsymbol{g}^j = (\boldsymbol{\nabla}_\mathrm{s}\boldsymbol{x}_0)^\mathrm{T}, \tag{17}$$

in analogy to Eq. (15). In all of the following, the Moore–Penrose inverse [22,23] of interfacial tensors will be denoted by $()^{-1}$. As a result of Eqs. (15) and (17),

$$\boldsymbol{F}_\mathrm{s}\cdot\boldsymbol{F}_\mathrm{s}^{-1} = \boldsymbol{I}_\mathrm{s}, \tag{18}$$

$$\boldsymbol{F}_\mathrm{s}^{-1}\cdot\boldsymbol{F}_\mathrm{s} = \boldsymbol{I}_{\mathrm{s},0}, \tag{19}$$

see also Eqs. (3) and (11). In addition, it can be shown that

$$\boldsymbol{\nabla}_{\mathrm{s},0} = \boldsymbol{g}_0^i\frac{\partial}{\partial\xi_i} = \boldsymbol{g}_0^i\boldsymbol{g}_i\cdot\boldsymbol{g}^j\frac{\partial}{\partial\xi_j} = \boldsymbol{F}_\mathrm{s}^\mathrm{T}\cdot\boldsymbol{\nabla}_\mathrm{s} \qquad \text{or equivalently,}$$

$$\boldsymbol{\nabla}_\mathrm{s} = \boldsymbol{F}_\mathrm{s}^{-\mathrm{T}}\cdot\boldsymbol{\nabla}_{\mathrm{s},0}, \tag{20}$$

where the superscript $()^{-\mathrm{T}}$ means taking both the inverse and the transpose of the corresponding tensor. To derive Eq. (20), which is also in accordance with Eqs. (15) and (18)–(19), we have used Eqs. (3), (12) and (15).

The interfacial Finger tensor $\boldsymbol{B}_\mathrm{s}$ is given by

$$\boldsymbol{B}_\mathrm{s} = \boldsymbol{F}_\mathrm{s}\cdot\boldsymbol{F}_\mathrm{s}^\mathrm{T} = g_0^{ij}\boldsymbol{g}_i\boldsymbol{g}_j, \tag{21}$$

where Eqs. (7) and (15) have been used. It can be seen that the directions of $\boldsymbol{B}_\mathrm{s}$ are tangential to the interface in the current configuration, since $\boldsymbol{g}_i$ are tangential vectors. If no deformation is applied, $\boldsymbol{B}_\mathrm{s}$ reduces to $\boldsymbol{B}_\mathrm{s}(t = t_0) = \boldsymbol{I}_{\mathrm{s},0}$ (see Eq. (11)). Eq. (21) shows that $\boldsymbol{B}_\mathrm{s} = \boldsymbol{B}_\mathrm{s}^\mathrm{T}$ is symmetric, and is a positive-definite interfacial tensor so that

$$\boldsymbol{a}\cdot\boldsymbol{B}_\mathrm{s}\cdot\boldsymbol{a} = (\boldsymbol{F}_\mathrm{s}^\mathrm{T}\cdot\boldsymbol{a})^2 > 0 \qquad \text{for all vectors } \boldsymbol{a} \text{ such that } \boldsymbol{I}_\mathrm{s}\cdot\boldsymbol{a} \neq \boldsymbol{0}. \tag{22}$$

As a consequence, one of the eigenvalues of $\boldsymbol{B}_\mathrm{s}$ equals zero with a corresponding eigenvector perpendicular to the interface (see Eq. (21)). The non-zero eigenvalues of $\boldsymbol{B}_\mathrm{s}$ are real and positive, and the corresponding eigenvectors can be chosen to be mutually perpendicular. It is shown in Appendix B.1 that

$$J_\mathrm{s} = \det_\mathrm{s}(\boldsymbol{F}_\mathrm{s}) = \lambda_1\lambda_2, \tag{23}$$

where λ_i, $i = 1,2$, are the square root of the non-zero eigenvalues of $\boldsymbol{B}_\mathrm{s}$.

Finally, using Eq. (6) and (17), $\boldsymbol{B}_\mathrm{s}^{-1}$ can be written as (see Eq. (21))

$$\boldsymbol{B}_\mathrm{s}^{-1} = \boldsymbol{F}_\mathrm{s}^{-\mathrm{T}} \cdot \boldsymbol{F}_\mathrm{s}^{-1} = g_{ij,0}\boldsymbol{g}^i\boldsymbol{g}^j. \tag{24}$$

It can then indeed be verified that $\boldsymbol{B}_\mathrm{s}^{-1}$ is the Moore–Penrose inverse [22,23] of $\boldsymbol{B}_\mathrm{s}$ such that $\boldsymbol{B}_\mathrm{s}^{-1} \cdot \boldsymbol{B}_\mathrm{s} = \boldsymbol{B}_\mathrm{s} \cdot \boldsymbol{B}_\mathrm{s}^{-1} = \boldsymbol{I}_\mathrm{s}$ (see Eqs. (3), (8), (11), (21) and (24)).

In summary, we have expressed interfacial equivalents of bulk deformation tensors, $\boldsymbol{F}_\mathrm{s}$ and $\boldsymbol{B}_\mathrm{s}$ (and their inverses), in terms of tangential vectors using curvilinear coordinates on the interface as described in Section 2.1. As will be explained later, these deformation tensors are the only kinematic quantities required for describing the constitutive behaviour of a general interfacial elastic solid, and are also useful in integral-type viscoelastic interface models.

2.2.2. Decomposition into elastic and plastic deformation

For describing the non-linear viscoelastic behaviour of interfaces, and in particular elastoviscoplasticity, it is useful to split the total deformation of the interface into its elastic and plastic parts. For this, we follow a successful approach for bulk materials by Lee et al. [24], which is applied also in [13,25]. By analogy to the bulk, we use the following decomposition of the surface deformation gradient tensor $\boldsymbol{F}_\mathrm{s}$,

$$\boldsymbol{F}_\mathrm{s} = \boldsymbol{F}_\mathrm{s,e} \cdot \boldsymbol{F}_\mathrm{s,p}, \tag{25}$$

with $\boldsymbol{F}_\mathrm{s,e}$ the elastic and $\boldsymbol{F}_\mathrm{s,p}$ the plastic part of $\boldsymbol{F}_\mathrm{s}$, which are functions of ξ and t. This decomposition is schematically depicted in Fig. 2, which for each ξ visualises the introduction of an intermediate planar configuration between the reference and current configurations. The tensor $\boldsymbol{F}_\mathrm{s,e}$ represents the elastic part of the deformation that is affected by infinitely rapid unloading in the current configuration, hence leaving the rate-dependent processes inactive, leading to the intermediate configuration. Note that the intermediate configuration is not a physical state the system reaches, and it cannot be described as a differentiable curved interface surface. An infinitesimal interface material line element in the intermediate configuration $d\boldsymbol{x}_\mathrm{I}$ after infinitely rapid unloading is determined by

$$d\boldsymbol{x}_\mathrm{I} = \boldsymbol{F}_\mathrm{s,e}^{-1} \cdot d\boldsymbol{x} = \boldsymbol{F}_\mathrm{s,e}^{-1} \cdot \boldsymbol{F}_\mathrm{s} \cdot d\boldsymbol{x}_0, \tag{26}$$

where $\boldsymbol{F}_\mathrm{s,e}^{-1}$ performs the inverse mapping of that by $\boldsymbol{F}_\mathrm{s,e}$. This intermediate configuration is therefore determined only by the plastic part of $\boldsymbol{F}_\mathrm{s}$, i.e. $d\boldsymbol{x}_\mathrm{I} = \boldsymbol{F}_\mathrm{s,p} \cdot d\boldsymbol{x}_0$, since $\boldsymbol{F}_\mathrm{s,p} = \boldsymbol{F}_\mathrm{s,e}^{-1} \cdot \boldsymbol{F}_\mathrm{s}$, see also Eq. (25). To make the multiplicative split in Eq. (25) unique, a constraint on the dynamics in the intermediate configuration must be imposed [25], which will be specified in Section 2.3.2. The elastic part of the relative change in interfacial surface area, analogous to that for the total deformation given by Eq. (16), reads

$$J_\mathrm{s,e} = \det_\mathrm{s}(\boldsymbol{F}_\mathrm{s,e}). \tag{27}$$

In summary, the surface deformation gradient tensor $\boldsymbol{F}_\mathrm{s}$ is decomposed into elastic and plastic parts by introduction of an intermediate configuration between the current and reference ones. Later in the paper, this will turn out to be convenient for describing non-linear viscoelastic behaviour.

2.3. Rate of deformation

2.3.1. Time derivative of surface deformation tensors

Taking the time derivative of Eq. (15), the evolution of $\boldsymbol{F}_\mathrm{s}$ is expressed as

$$\dot{\boldsymbol{F}}_\mathrm{s} = \boldsymbol{L}_\mathrm{s} \cdot \boldsymbol{F}_\mathrm{s}, \tag{28}$$

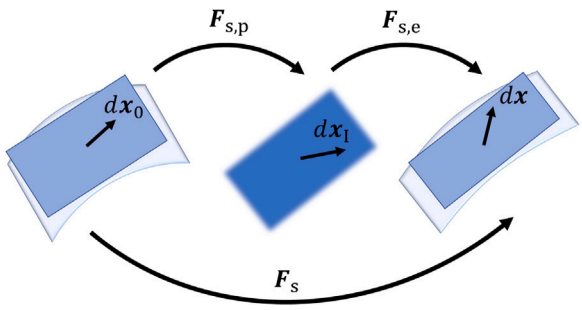

Fig. 2. Schematic representation of the multiplicative decomposition of the total surface deformation gradient tensor $\boldsymbol{F}_\mathrm{s}$ into an elastic part $\boldsymbol{F}_\mathrm{s,e}$ and a plastic part $\boldsymbol{F}_\mathrm{s,p}$, for given ξ, with an intermediate configuration between the reference and current configurations, see also Eq. (25).

where we define the material derivative as

$$\dot{()} = \left.\frac{\partial()}{\partial t}\right|_\xi, \tag{29}$$

which is the time rate of change of a quantity following the motion of an interface particle [21]. In all of the following, $()^\cdot$ denotes the material derivative of the expression between parentheses. The surface velocity gradient tensor $\boldsymbol{L}_\mathrm{s}$ appearing in Eq. (28) is given by

$$\boldsymbol{L}_\mathrm{s} = (\boldsymbol{\nabla}_\mathrm{s}\boldsymbol{u})^\mathrm{T}, \tag{30}$$

with $\boldsymbol{u} = \dot{\boldsymbol{x}}$ the velocity vector at the interface. Eq. (28) is obtained by substituting the time derivative of the base vectors $\boldsymbol{g}_i$, see Appendix B.2. Note that $\boldsymbol{L}_\mathrm{s}$ may have out-of-plane directions on its left-hand side, since $\boldsymbol{u}$ is the full velocity vector and not just the tangential part. However, the surface-gradient 'direction' of $\boldsymbol{L}_\mathrm{s}$, i.e. its right-hand side, is tangential to the interface, see also Eq. (12). Therefore, projection of $\boldsymbol{L}_\mathrm{s}$ onto the interface is only effective if the product with $\boldsymbol{I}_\mathrm{s}$ is performed from the velocity 'direction' side of $\boldsymbol{L}_\mathrm{s}$. Hence, $\boldsymbol{L}_\mathrm{s} \cdot \boldsymbol{I}_\mathrm{s} = \boldsymbol{L}_\mathrm{s}$ and $\boldsymbol{I}_\mathrm{s} \cdot \boldsymbol{L}_\mathrm{s}^\mathrm{T} = \boldsymbol{L}_\mathrm{s}^\mathrm{T}$ leave $\boldsymbol{L}_\mathrm{s}$ and $\boldsymbol{L}_\mathrm{s}^\mathrm{T}$ unchanged, however, in contrast, $\boldsymbol{I}_\mathrm{s} \cdot \boldsymbol{L}_\mathrm{s} \neq \boldsymbol{L}_\mathrm{s}$ and $\boldsymbol{L}_\mathrm{s}^\mathrm{T} \cdot \boldsymbol{I}_\mathrm{s} \neq \boldsymbol{L}_\mathrm{s}^\mathrm{T}$ in general, see also Eq. (12).

By differentiating Eq. (16) with respect to time using the chain rule for differentiation, the relative time rate of change of the interfacial surface area $\dot{J}_\mathrm{s}/J_\mathrm{s}$ is obtained (see Appendix B.4):

$$\frac{\dot{J}_\mathrm{s}}{J_\mathrm{s}} = \mathrm{tr}(\boldsymbol{D}_\mathrm{s}), \tag{31}$$

with the surface rate-of-deformation tensor defined by

$$\boldsymbol{D}_\mathrm{s} = \frac{1}{2}(\boldsymbol{I}_\mathrm{s} \cdot \boldsymbol{L}_\mathrm{s} + \boldsymbol{L}_\mathrm{s}^\mathrm{T} \cdot \boldsymbol{I}_\mathrm{s}). \tag{32}$$

It is not necessary to write Eq. (31) in terms of $\boldsymbol{D}_\mathrm{s}$ but we choose to define $\boldsymbol{D}_\mathrm{s}$ here since it will be used throughout the paper. Note that the directions of $\boldsymbol{D}_\mathrm{s}$ are tangential to the interface because of the projections with $\boldsymbol{I}_\mathrm{s}$.

The evolution of the interfacial Finger tensor $\boldsymbol{B}_\mathrm{s} = \boldsymbol{F}_\mathrm{s} \cdot \boldsymbol{F}_\mathrm{s}^\mathrm{T}$ is straightforward to write down using the product rule for differentiation and Eq. (28):

$$\dot{\boldsymbol{B}}_\mathrm{s} = \boldsymbol{L}_\mathrm{s} \cdot \boldsymbol{B}_\mathrm{s} + \boldsymbol{B}_\mathrm{s} \cdot \boldsymbol{L}_\mathrm{s}^\mathrm{T}, \tag{33}$$

or similarly,

$$\overset{\triangledown}{\boldsymbol{B}}_\mathrm{s} = \boldsymbol{0}, \tag{34}$$

with the surface upper-convected derivative $\overset{\triangledown}{()}$ defined by

$$\overset{\triangledown}{()} = \dot{()} - \boldsymbol{L}_\mathrm{s} \cdot () - () \cdot \boldsymbol{L}_\mathrm{s}^\mathrm{T}. \tag{35}$$

The notation $()^\triangledown$ will be used for the surface upper-convected derivative of expressions between parentheses. It can be proven that $\overset{\triangledown}{\boldsymbol{A}}_\mathrm{s} = \overset{\triangledown}{A}_\mathrm{s}^{ij}\boldsymbol{g}_i\boldsymbol{g}_j$ for an arbitrary tensor $\boldsymbol{A}_\mathrm{s} = A_\mathrm{s}^{ij}\boldsymbol{g}_i\boldsymbol{g}_j$ tangential to the interface, by

applying the product rule for differentiation to $\boldsymbol{A}_s$ and then substituting Eq. (B.6) (see Appendix B.2 for details). This shows that the surface upper-convected derivative keeps $\boldsymbol{A}_s$ tangential, since the time rate of change of $\boldsymbol{A}_s$ is tangential at all times. Therefore, using the surface upper-convected derivative as the time derivative in a constitutive equation ensures the interfacial stress tensor to remain tangential to the interface, as long as the other terms in the constitutive equation (when added together) are also tangential to the interface. By applying Eq. (35) to $\boldsymbol{I}_s$, it turns out that (see Appendix B.3)

$$\overset{\nabla}{\boldsymbol{I}}_s = -2\boldsymbol{D}_s. \tag{36}$$

This result is similar to that for the upper-convected derivative of the unit tensor in bulk rheology, but $\boldsymbol{D}_s$ is the projected rate-of-deformation tensor on the interface, see Eq. (32).

The evolution equation for $\boldsymbol{F}_s^{-1}$, obtained by differentiating Eq. (18) with respect to time using the product rule for differentiation, then substituting Eqs. (28) and (B.9) and rearranging terms, reads

$$(\boldsymbol{F}_s^{-1})^{\bullet} = -\boldsymbol{F}_s^{-1}\cdot(2\boldsymbol{D}_s - \boldsymbol{L}_s^{\mathrm{T}}). \tag{37}$$

The dynamics of $\boldsymbol{B}_s^{-1}$ are now obtained by applying the product rule for differentiation to Eq. (24) and substituting Eq. (37):

$$(\boldsymbol{B}_s^{-1})^{\bullet} = -(2\boldsymbol{D}_s - \boldsymbol{L}_s)\cdot\boldsymbol{B}_s^{-1} - \boldsymbol{B}_s^{-1}\cdot(2\boldsymbol{D}_s - \boldsymbol{L}_s^{\mathrm{T}}). \tag{38}$$

Eq. (38) can alternatively be written as

$$(\boldsymbol{B}_s^{-1})^{\overset{\Delta}{}} = \boldsymbol{0}, \tag{39}$$

with the surface lower-convected derivative $\overset{\Delta}{()}$ given by

$$\overset{\Delta}{()} = \dot{()} + (2\boldsymbol{D}_s - \boldsymbol{L}_s)\cdot() + ()\cdot(2\boldsymbol{D}_s - \boldsymbol{L}_s^{\mathrm{T}}). \tag{40}$$

The notation $()^{\overset{\Delta}{}}$ will be used for the surface lower-convected derivative of expressions between parentheses. It can be proven that $\overset{\Delta}{\boldsymbol{A}}_s = \dot{A}_{s,ij}\boldsymbol{g}^i\boldsymbol{g}^j$ for an arbitrary tensor $\boldsymbol{A}_s = A_{s,ij}\boldsymbol{g}^i\boldsymbol{g}^j$ tangential to the interface, by first substituting Eq. (10) and then applying the product rule for differentiation and substituting Eq. (B.8) (see Appendix B.2 for details). This shows that the surface lower-convected derivative keeps $\boldsymbol{A}_s$ tangential, since the time rate of change of $\boldsymbol{A}_s$ is tangential. Therefore, using the surface lower-convected derivative as the time derivative in a constitutive equation ensures the interfacial stress tensor to remain tangential to the interface, as long as the other terms in the constitutive equation (when added together) are also tangential to the interface. It can furthermore be shown that

$$\overset{\Delta}{\boldsymbol{I}}_s = 2\boldsymbol{D}_s, \tag{41}$$

by applying Eq. (40) to $\boldsymbol{I}_s$ and substituting the expression for $\dot{\boldsymbol{I}}_s$ from Eq. (B.9).

The surface convected derivatives defined on interfaces in Eqs. (35) and (40) are non-trivial generalisations of the convected derivatives defined in the bulk [26]. The surface upper-convected derivative reduces to that for the bulk if $\boldsymbol{L}_s = \boldsymbol{L}$ at the interface, with $\boldsymbol{L}$ the transposed bulk velocity gradient tensor. The surface lower-convected derivative reduces to that for the bulk if $2\boldsymbol{D}_s - \boldsymbol{L}_s = \boldsymbol{L}^{\mathrm{T}}$ at the interface. Examples of such flows are planar shear and dilatational deformation of an interface. Moreover, note that both surface-convected derivative operators in Eqs. (35) and (40) applied to an arbitrary interfacial tensor yield an expression containing individual tensor terms with, in general, out-of-plane directions. However, these terms added together yield a tensor tangential to the interface, as shown in the text below Eqs. (35) and (40). This ensures objectivity, keeping an interfacial tensor tangential to the interface in the course of time. In contrast, the material derivative in Eq. (29) of an interfacial tensor is in general not a tangential tensor, since the directions of such a tensor, e.g. the interfacial stress tensor, rotate along with the interface.

In summary, the evolution equations for the surface deformation tensors $\boldsymbol{F}_s$, $\boldsymbol{B}_s$ (and their inverses) have been derived. This does not only allow for a transient description of elastic solid and integral-type viscoelastic interface behaviour, but the surface velocity gradient tensor and the surface upper- and lower-convected derivatives, helpful in the formulation of differential viscoelastic interface models, naturally appear as a result. For a more general objective time derivative for interfaces, one could introduce an interface version of the Gordon–Schowalter time derivative, in analogy to the bulk [27–29].

2.3.2. Decomposition in elastic and plastic deformation

The evolution equation for $\boldsymbol{F}_{s,e}$, the elastic part of the surface deformation gradient tensor $\boldsymbol{F}_s$, can be obtained by rewriting the evolution of Eq. (25) using the product rule for differentiation and substituting Eq. (28). It is derived in detail in Appendix B.5; the result is (see [13,25] for the case of bulk)

$$\dot{\boldsymbol{F}}_{s,e}\cdot\boldsymbol{I}_{s,I} = (\boldsymbol{L}_s - \boldsymbol{L}_{s,p})\cdot\boldsymbol{F}_{s,e}, \tag{42}$$

with $\boldsymbol{I}_{s,I}$ the surface unit tensor in the intermediate configuration. Furthermore, we have defined

$$\boldsymbol{L}_{s,p} = \boldsymbol{F}_{s,e}\cdot\dot{\boldsymbol{F}}_{s,p}\cdot\boldsymbol{F}_{s,p}^{-1}\cdot\boldsymbol{F}_{s,e}^{-1}, \tag{43}$$

the plastic counterpart of $\boldsymbol{L}_s$ in the current configuration, for which a constitutive equation will be specified later. It can be seen from Eq. (43) that $\boldsymbol{L}_{s,p}$ is a tensor with directions in the plane of the interface in the current configuration, as the directions of $\boldsymbol{F}_{s,e}$ on its left-hand side and those of $\boldsymbol{F}_{s,e}^{-1}$ on its right-hand side are tangential to the interface in the current configuration. This is because $\boldsymbol{F}_{s,e}$ and $\boldsymbol{F}_{s,e}^{-1}$ map infinitesimal interface line elements between the intermediate and current configurations, see Eq. (26). Therefore, projection of $\boldsymbol{L}_{s,p}$ onto the interface as for $\boldsymbol{D}_s$ in Eq. (32) is not required, since $\boldsymbol{L}_{s,p}$ is already an in-plane tensor. For the relative time rate of change of the elastic part of the relative change in interfacial surface area, by analogy to Eq. (31) we write

$$\frac{\dot{J}_{s,e}}{J_{s,e}} = \mathrm{tr}(\boldsymbol{D}_s - \boldsymbol{D}_{s,p}), \tag{44}$$

with $\boldsymbol{D}_{s,p} = (\boldsymbol{L}_{s,p} + \boldsymbol{L}_{s,p}^{\mathrm{T}})/2$ the plastic surface rate-of-deformation tensor for which a constitutive equation will be specified in the following. For deriving Eq. (44), a similar calculation can be performed as for Eq. (31) in Appendix B.4, using also Appendix B.5 to describe the intermediate configuration. Note that $\boldsymbol{I}_{s,I}$, although being present in Eq. (42) and appearing in intermediate steps of the calculation, is absent from the final result in Eq. (44).

The evolution equation for the elastic part of the interfacial Finger tensor

$$\boldsymbol{B}_{s,e} = \boldsymbol{F}_{s,e}\cdot\boldsymbol{F}_{s,e}^{\mathrm{T}}, \tag{45}$$

can be written down by applying the product rule for differentiation to Eq. (45), and then substituting Eqs. (42) and (45). In doing so, we assume that plastic deformation occurs spin-free since for isotropic materials the orientation in the intermediate configuration is irrelevant [30], which results in a vanishing plastic surface spin tensor $\boldsymbol{\Omega}_{s,p} = (\boldsymbol{L}_{s,p} - \boldsymbol{L}_{s,p}^{\mathrm{T}})/2 = \boldsymbol{0}$, see Eq. (43). This makes the evolution of $\boldsymbol{B}_{s,e}$ unique, given a constitutive equation for $\boldsymbol{D}_{s,p}$. Using $\boldsymbol{L}_{s,p} = \boldsymbol{D}_{s,p} + \boldsymbol{\Omega}_{s,p} = \boldsymbol{D}_{s,p}$, this choice results in (see [30] for the case of bulk)

$$\dot{\boldsymbol{B}}_{s,e} = (\boldsymbol{L}_s - \boldsymbol{D}_{s,p})\cdot\boldsymbol{B}_{s,e} + \boldsymbol{B}_{s,e}\cdot(\boldsymbol{L}_s^{\mathrm{T}} - \boldsymbol{D}_{s,p}), \tag{46}$$

or equivalently,

$$\overset{\nabla}{\boldsymbol{B}}_{s,e} = -(\boldsymbol{D}_{s,p}\cdot\boldsymbol{B}_{s,e} + \boldsymbol{B}_{s,e}\cdot\boldsymbol{D}_{s,p}). \tag{47}$$

Note, that $\boldsymbol{I}_{s,I}$ appearing in Eq. (42) is absent from Eqs. (46)–(47) eventually. By comparing Eqs. (46)–(47) with Eqs. (33)–(34), it can be seen that relaxation of the elastic deformation comes with non-zero plastic deformation (rate) $\boldsymbol{D}_{s,p}$.

The evolution equation for $\boldsymbol{F}_{\mathrm{s,e}}^{-1}$ is obtained by applying the product rule for differentiation to $\boldsymbol{F}_{\mathrm{s,e}} \cdot \boldsymbol{F}_{\mathrm{s,e}}^{-1} = \boldsymbol{I}_{\mathrm{s}}$, substituting Eqs. (B.9) and (42)–(43), and rearranging terms, resulting in

$$\boldsymbol{I}_{\mathrm{s,I}} \cdot (\boldsymbol{F}_{\mathrm{s,e}}^{-1})^{\bullet} = \boldsymbol{F}_{\mathrm{s,e}}^{-1} \cdot \left(\boldsymbol{L}_{\mathrm{s,p}} - (2\boldsymbol{D}_{\mathrm{s}} - \boldsymbol{L}_{\mathrm{s}}^{\mathrm{T}})\right). \tag{48}$$

The inverse of the elastic part of the interfacial Finger tensor $\boldsymbol{B}_{\mathrm{s,e}}^{-1}$ is given by $\boldsymbol{B}_{\mathrm{s,e}}^{-1} = \boldsymbol{F}_{\mathrm{s,e}}^{-\mathrm{T}} \cdot \boldsymbol{F}_{\mathrm{s,e}}^{-1}$ (see Eq. (45)). The evolution equation of $\boldsymbol{B}_{\mathrm{s,e}}^{-1}$ then follows from applying the product rule for differentiation and substitution of Eq. (48), and can be written as

$$(\boldsymbol{B}_{\mathrm{s,e}}^{-1})^{\bullet} = \left(\boldsymbol{D}_{\mathrm{s,p}} - (2\boldsymbol{D}_{\mathrm{s}} - \boldsymbol{L}_{\mathrm{s}})\right) \cdot \boldsymbol{B}_{\mathrm{s,e}}^{-1} + \boldsymbol{B}_{\mathrm{s,e}}^{-1} \cdot \left(\boldsymbol{D}_{\mathrm{s,p}} - (2\boldsymbol{D}_{\mathrm{s}} - \boldsymbol{L}_{\mathrm{s}}^{\mathrm{T}})\right), \tag{49}$$

or equivalently,

$$(\boldsymbol{B}_{\mathrm{s,e}}^{-1})^{\Delta} = \boldsymbol{D}_{\mathrm{s,p}} \cdot \boldsymbol{B}_{\mathrm{s,e}}^{-1} + \boldsymbol{B}_{\mathrm{s,e}}^{-1} \cdot \boldsymbol{D}_{\mathrm{s,p}}, \tag{50}$$

where we have again used that $\boldsymbol{L}_{\mathrm{s,p}} = \boldsymbol{D}_{\mathrm{s,p}}$, since rotations in the intermediate configuration are irrelevant for isotropic interface materials [25,30]. Also note, that $\boldsymbol{I}_{\mathrm{s,I}}$ appearing in Eq. (48) is absent from Eqs. (49)–(50) eventually. Comparison of Eq. (49)–(50) with Eqs. (38)–(39) shows that relaxation of the elastic deformation comes with non-zero plastic deformation (rate) $\boldsymbol{D}_{\mathrm{s,p}}$.

In summary, evolution equations have been derived for the elastic part of surface deformation tensors, $\boldsymbol{F}_{\mathrm{s,e}}$ and $\boldsymbol{B}_{\mathrm{s,e}}$ (and their inverses). If these evolution equations are complemented by appropriate constitutive equations for the plastic surface rate-of-deformation tensor $\boldsymbol{D}_{\mathrm{s,p}}$ and interfacial stress tensor $\boldsymbol{\tau}_{\mathrm{s}}$, they enable the formulation of constitutive models for non-linear viscoelastic interfaces with upper- and lower-convected behaviour. This will be treated in the next sections.

3. Constitutive modelling

3.1. Mechanical representation

We will present a framework for the formulation of constitutive models to describe rheologically complex, i.e. non-linear viscoelastic, interface behaviour; in particular quasi-linear viscoelasticity and elastoviscoplasticity. The latter type of material behaviour is characterised by a primarily elastic response at small deformations during a step strain-rate experiment, with only minor viscous effects. Upon further deformation and build up of elastic stress, a gradual but rather sharp transition from elastic to predominantly viscous behaviour occurs when the stress approaches the (dynamic) yield stress. At the yield point, the stress attains either a maximum or a plateau value and the material flows, i.e. it deforms plastically. Upon even further deformation, the stress remains constant (plateau) or decreases (strain softening), after which it will become stationary. Depending on whether the interfacial microstructural environment is more solid or fluid like, additional elastic and/or viscous stresses are present due to interfacial flow, and the microstructure will/will not return to its undeformed configuration after cessation of flow.

The type of material behaviour discussed in this section is commonly described in the case of bulk materials by so-called 'generalised Maxwell models' [30]. In qualitative terms it represents a mechanical model consisting of a combination of springs and dashpots linked in series and in parallel. The mechanical analogue of this broad collection of models is schematically depicted in Fig. 3. A combination of n parallel Maxwell elements is connected to a spring and a dashpot in parallel. The Maxwell element consists of a spring and a dashpot linked in series; the stresses in the spring and in the dashpot are equal and their strain rates are additive. The interfacial rate of deformation equals the deformation rate in each of the parallel elements. The total interfacial stress $\boldsymbol{\tau}_{\mathrm{s}}$ is the sum over the stresses in each parallel element and can in general be written as

$$\boldsymbol{\tau}_{\mathrm{s}} = \boldsymbol{\tau}_{\mathrm{s,ve}} + \boldsymbol{\tau}_{\mathrm{s,e}} + \boldsymbol{\tau}_{\mathrm{s,v}}, \tag{51}$$

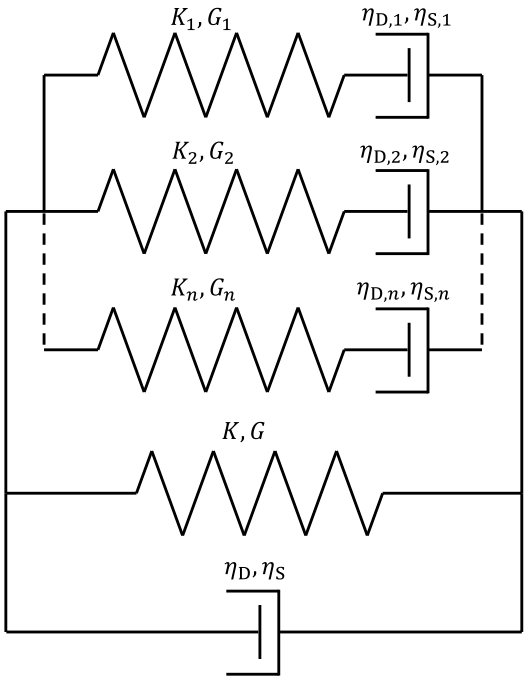

Fig. 3. Mechanical analogue of a framework for non-linear viscoelastic models for interfaces. A combination of n parallel Maxwell elements, consisting of an elastic spring connected in series to a viscous dashpot, is linked to both a spring and a dashpot in parallel. Material parameters K and G are interfacial elastic moduli and η_{D} and η_{S} are interfacial viscosities for shear and dilatation, respectively.

where $\boldsymbol{\tau}_{\mathrm{s,e}}$ is the elastic stress in the parallel spring, $\boldsymbol{\tau}_{\mathrm{s,v}}$ is the viscous stress in the parallel dashpot, and the viscoelastic stress $\boldsymbol{\tau}_{\mathrm{s,ve}}$ of the combined parallel Maxwell elements is given by

$$\boldsymbol{\tau}_{\mathrm{s,ve}} = \sum_{i=1}^{n} \boldsymbol{\tau}_{\mathrm{s,ve},i}, \tag{52}$$

where $\boldsymbol{\tau}_{\mathrm{s,ve},i}$ is the viscoelastic stress in Maxwell element i. For the viscous and elastic stresses in the parallel dashpot and spring, one can use the Boussinesq–Scriven viscous interface model [12] and a Neo-Hookean type hyperelastic interface model, for example (a part of) the interfacial Hütter–Tervoort model [13,14], respectively. The parallel dashpot and spring are only suggested but will not be considered in this paper. The parallel spring can for instance be used to include post-yield strain hardening as already done for bulk (see [31–33]). In the following, we will only consider a single Maxwell element, although the extension to multiple elements is straightforward. Therefore, we will drop the subscripts i and write $\boldsymbol{\tau}_{\mathrm{s}}$ for the viscoelastic stress $\boldsymbol{\tau}_{\mathrm{s,ve},i}$ for the ease of notation.

To relate interfacial stress to deformation (rate) for the generalised Maxwell element, we make use of the interface kinematics as described in Section 2. A constitutive equation for the plastic surface rate-of-deformation tensor $\boldsymbol{D}_{\mathrm{s,p}}$, a measure for the deformation rate of the dashpot, is required to solve Eq. (46) for $\boldsymbol{B}_{\mathrm{s,e}}$ and Eq. (49) for $\boldsymbol{B}_{\mathrm{s,e}}^{-1}$, which are measures for the elastic deformation of the spring. Hence, these tensors can be considered as structural variables. Furthermore, a constitutive relation between the interfacial stress tensor $\boldsymbol{\tau}_{\mathrm{s}}$ and the elastic deformation is needed. This will be the subject of the next sections.

3.2. General equations

For the constitutive equation for the plastic interfacial rate-of-deformation tensor $\boldsymbol{D}_{\mathrm{s,p}}$, we assume that in the Maxwell element, plastic deformation (of the dashpot) is driven by interfacial stress (in

the spring), see also [30–34] for the case of bulk. For $\boldsymbol{\tau}_s$ we use interfacial equivalents of hyperelastic solid models similar to the Neo-Hookean model for bulk, which are expressed in terms of powers of the elastic part of the interfacial Finger tensor, $\boldsymbol{B}_{s,e}$, and invariants. To keep the mathematical formulation of our subset of models more general, the constitutive equation for $\boldsymbol{D}_{s,p}$ will also be expressed in terms of powers of $\boldsymbol{B}_{s,e}$ and its principal invariants

$$J_1(\boldsymbol{B}_{s,e}) = \mathrm{tr}(\boldsymbol{B}_{s,e}), \qquad J_2(\boldsymbol{B}_{s,e}) = \tfrac{1}{2}(\mathrm{tr}(\boldsymbol{B}_{s,e})^2 - \mathrm{tr}(\boldsymbol{B}_{s,e}^2)). \tag{53}$$

Note that $J_2(\boldsymbol{B}_{s,e}) = J_{s,e}^2$, see Eq. (23), which also holds for the elastic part of the deformation. In the following, we will write J_1 and J_2 for the invariants of $\boldsymbol{B}_{s,e}$ for the ease of notation. However, for an arbitrary other tensor $\boldsymbol{A}_s$ we will use the notation $J_1(\boldsymbol{A}_s)$ and $J_2(\boldsymbol{A}_s)$. The Cayley–Hamilton theorem applied to $\boldsymbol{B}_{s,e}$, which is a rank-2 interfacial tensor with determinant $J_3(\boldsymbol{B}_{s,e}) = \det(\boldsymbol{B}_{s,e}) = 0$, after multiplication with $\boldsymbol{B}_{s,e}^{-1}$, reduces to

$$\boldsymbol{B}_{s,e}^2 - J_1\boldsymbol{B}_{s,e} + J_2\boldsymbol{I}_s = \boldsymbol{0}, \tag{54}$$

showing that two subsequent powers of $\boldsymbol{B}_{s,e}$, e.g. the pair $\boldsymbol{B}_{s,e}$ and $\boldsymbol{I}_s$, or $\boldsymbol{I}_s$ and $\boldsymbol{B}_{s,e}^{-1}$, suffice for calculating any other power of $\boldsymbol{B}_{s,e}$. To distinguish between plastic deformation of the interface at constant shape but changing surface area, and at constant surface area but changing shape, the tensor $\boldsymbol{D}_{s,p}$ can be uniquely split as

$$\boldsymbol{D}_{s,p} = \boldsymbol{D}_{s,p}^{h} + \boldsymbol{D}_{s,p}^{d}, \tag{55}$$

with hydrostatic part $\boldsymbol{D}_{s,p}^{h} = \frac{1}{2}\mathrm{tr}(\boldsymbol{D}_{s,p})\boldsymbol{I}_s$ and deviatoric part $\boldsymbol{D}_{s,p}^{d} = \boldsymbol{D}_{s,p} - \boldsymbol{D}_{s,p}^{h}$. Using Eq. (54), $\boldsymbol{D}_{s,p}$ can in general be expressed in terms of $\boldsymbol{I}_s$ and $\boldsymbol{B}_{s,e}$ and invariants as

$$\boldsymbol{D}_{s,p}^{h} = \frac{1}{2\lambda_D(J_1,J_2,J_s)}\boldsymbol{I}_s, \qquad \boldsymbol{D}_{s,p}^{d} = \frac{1}{2\lambda_S(J_1,J_2,J_s)}\bar{\boldsymbol{B}}_{s,e}^{d}, \tag{56}$$

with $\bar{\boldsymbol{B}}_{s,e}^{d} = \bar{\boldsymbol{B}}_{s,e} - \frac{1}{2}J_1(\bar{\boldsymbol{B}}_{s,e})\boldsymbol{I}_s$ the deviatoric part of $\bar{\boldsymbol{B}}_{s,e}$. The tensor $\boldsymbol{D}_{s,p}^{d}$ is expressed for later convenience in terms of $\bar{\boldsymbol{B}}_{s,e}^{d}$, with $\bar{\boldsymbol{B}}_{s,e}$ the isochoric part of $\boldsymbol{B}_{s,e}$, i.e. $\bar{\boldsymbol{B}}_{s,e} = (1/J_{s,e})\boldsymbol{B}_{s,e}$ so that $\det_s(\bar{\boldsymbol{B}}_{s,e}) = 1$. The coefficients λ_D and λ_S are the interfacial dilatational and shear relaxation times, respectively, which are functions of the invariants of $\boldsymbol{B}_{s,e}$ and of J_s; the dependence on J_s will be explained below. Later in this paper it will be shown why λ_D and λ_S are called relaxation times for dilatation and shear, respectively. For practical use, however, specific choices for the relaxation speeds $1/\lambda_D$ and $1/\lambda_S$ will be presented. Eqs. (46) or (47) and (56) now form a closed set of equations in terms of the internal deformation variable or structural variable $\boldsymbol{B}_{s,e}$, the relative change in surface area J_s, and the external deformation-rate tensor $\boldsymbol{L}_s$. External/internal variable here means macroscopically observable/unobservable quantity, respectively. For a closed form of Eq. (49) or (50), it would be more convenient to express $\boldsymbol{D}_{s,p}$ in terms of $\boldsymbol{I}_s$ and $\boldsymbol{B}_{s,e}^{-1}$ and invariants thereof. However, we will not use that in this paper.

In addition, a constitutive equation for the interfacial stress $\boldsymbol{\tau}_s$ is required. To this end, we assume that the stress in the Maxwell element (see Fig. 3) results from the deformation of the elastic spring, for which the structural variables $\boldsymbol{B}_{s,e}$ and $\boldsymbol{B}_{s,e}^{-1}$ are measures. Therefore, we will use hyperelastic interface constitutive equations for $\boldsymbol{\tau}_s$ that are defined in terms of the Helmholtz free energy per unit area in the current configuration, ψ_s. For isotropic interface materials, ψ_s is in general a function of the invariants of $\boldsymbol{B}_{s,e}$ (or of $\boldsymbol{B}_{s,e}^{-1}$, which can be obtained from those of $\boldsymbol{B}_{s,e}$), and of J_s to describe the change in the amount of interfacial area upon deformation. The latter is included as an independent variable, since it cannot be obtained from the surface determinant of $\boldsymbol{B}_{s,e}$, because generally $\boldsymbol{D}_{s,p}^{h} \neq \boldsymbol{0}$ [13,35], and therefore $J_{s,e} \neq J_s$ (see Eqs. (31) and (44)). Including J_s as a separate variable would not have been required if either the total interfacial Finger tensor $\boldsymbol{B}_s$ (or its inverse $\boldsymbol{B}_s^{-1}$) was used to describe the deformation [35], or if $\boldsymbol{B}_{s,e}$ (or $\boldsymbol{B}_{s,e}^{-1}$) was used while plastic deformation was incompressible ($\boldsymbol{D}_{s,p}^{h} = \boldsymbol{0}$) [13], since J_s could then be obtained indirectly based on these quantities. The Helmholtz free energy area density ψ_s can now be written as $\psi_s = \psi_s(J_1, J_2, J_s)$, where J_1 and J_2 are the principal invariants of $\boldsymbol{B}_{s,e}$ (see Eq. (53)). Using nonequilibrium thermodynamics arguments, it can be shown that the following expression for the interfacial stress holds (see Appendix B.6 for the derivation) [29,36–38]:

$$\boldsymbol{\tau}_s = \frac{\partial\hat{\psi}_s}{\partial J_s}\boldsymbol{I}_s + \boldsymbol{\tau}_{s,c}, \tag{57}$$

with $\boldsymbol{\tau}_{s,c}$ given by

$$\boldsymbol{\tau}_{s,c} = \begin{cases} \dfrac{2}{J_s}\boldsymbol{B}_{s,e}\cdot\dfrac{\partial\hat{\psi}_s}{\partial\boldsymbol{B}_{s,e}}, & \text{if } \boldsymbol{B}_{s,e} \text{ is the structural variable} \\ & \text{of choice with Eq. (47),} \\ -\dfrac{2}{J_s}\boldsymbol{B}_{s,e}^{-1}\cdot\dfrac{\partial\hat{\psi}_s}{\partial\boldsymbol{B}_{s,e}^{-1}}, & \text{if } \boldsymbol{B}_{s,e}^{-1} \text{ is the structural variable} \\ & \text{of choice with Eq. (50),} \end{cases} \tag{58}$$

where $\hat{\psi}_s = J_s\psi_s$ is the interfacial Helmholtz free energy density per unit area in the reference configuration. Note that the expressions for $\boldsymbol{\tau}_{s,c}$ in Eq. (58) are equivalent.[1] About Eq. (58), it is particularly pointed out that $\boldsymbol{\tau}_{s,c}$ contains the prefactor $1/J_s$, rather than $1/J_{s,e}$, which is in analogy to the treatment for 3D bulk materials (e.g., see [13]). However, in 3D bulk materials, one typically assumes that the viscoplastic deformation is incompressible, which leads to $J_{s,e} = J_s$, and so this subtlety is irrelevant for all practical purposes. In contrast, viscoplastic deformation of interfaces may *not* be assumed to be incompressible, and therefore attention must be paid at not taking J_s and $J_{s,e}$ equivalent to each other.

The interfacial stress tensor in Eq. (57) can be rewritten using the chain rule for differentiation, $\partial J_1/\partial\boldsymbol{B}_{s,e} = \boldsymbol{I}_s$ and $\partial J_2/\partial\boldsymbol{B}_{s,e} = J_2\boldsymbol{B}_{s,e}^{-1}$, and Eqs. (53)–(54), as

$$\begin{aligned}\boldsymbol{\tau}_s &= \frac{\partial\hat{\psi}_s}{\partial J_s}\boldsymbol{I}_s + \frac{2}{J_s}\boldsymbol{B}_{s,e}\cdot\frac{\partial\hat{\psi}_s}{\partial\boldsymbol{B}_{s,e}} \\ &= \frac{\partial\hat{\psi}_s}{\partial J_s}\boldsymbol{I}_s + \frac{2}{J_s}\boldsymbol{B}_{s,e}\cdot\left(\frac{\partial\hat{\psi}_s}{\partial J_1}\frac{\partial J_1}{\partial\boldsymbol{B}_{s,e}} + \frac{\partial\hat{\psi}_s}{\partial J_2}\frac{\partial J_2}{\partial\boldsymbol{B}_{s,e}}\right) \\ &= a_D(J_1,J_2,J_s)\boldsymbol{I}_s + a_S(J_1,J_2,J_s)\bar{\boldsymbol{B}}_{s,e}^{d},\end{aligned} \tag{59}$$

with a_D and a_S two functions, and where we choose to express the second term in $\boldsymbol{\tau}_s$ in terms of $\bar{\boldsymbol{B}}_{s,e}^{d}$ for later convenience. Hence, $\boldsymbol{\tau}_s$ can be expressed in terms of powers of $\boldsymbol{B}_{s,e}$ and its invariants (see Eqs. (53)–(54)), and in terms of J_s. Eq. (59) is the constitutive equation for the stress in the Maxwell element. Eq. (59) can also be used to describe the stress of a general interfacial solid that behaves purely elastically, by replacing $\boldsymbol{B}_{s,e}$ by $\boldsymbol{B}_s$ and deleting the $(\partial\hat{\psi}_s/\partial J_s)$-contribution (to avoid double-counting). In the following, we limit ourselves to models for which ψ_s (and hence also $\boldsymbol{\tau}_s$) is proportional to $1/J_s$ (e.g. rubber elasticity) and hence $\hat{\psi}_s$ is independent of J_s. This means that the stress tensor given in Eq. (57) reduces to $\boldsymbol{\tau}_{s,c}$ from Eq. (58): $\boldsymbol{\tau}_s = \boldsymbol{\tau}_{s,c}$; in general, however, additional isotropic terms would need to be included in $\boldsymbol{\tau}_s$ [36], as can be seen in the first term of Eq. (57).

The thermodynamic consistency of our framework is proven in Appendix B.6 by calculating, beyond the expression for the interfacial stress tensor in Eqs. (57)–(58), the interfacial entropy-production rate for the irreversible dynamics. This yields the following condition on the relation between $\boldsymbol{\tau}_{s,c}$ and $\boldsymbol{D}_{s,p}$ to be fulfilled [29,36]:

$$\boldsymbol{\tau}_{s,c} : \boldsymbol{D}_{s,p} \geq 0, \tag{60}$$

[1] This can be shown by writing $\boldsymbol{\tau}_{s,c} = (2/J_s)\boldsymbol{B}_{s,e}\cdot\partial\hat{\psi}_s/\partial\boldsymbol{B}_{s,e}^{-1} : \partial\boldsymbol{B}_{s,e}^{-1}/\partial\boldsymbol{B}_{s,e}$, applying the chain rule for differentiation, and then substituting the expression for $\partial\boldsymbol{B}_{s,e}^{-1}/\partial\boldsymbol{B}_{s,e}$ obtained by applying the product rule for differentiation to $\partial(\boldsymbol{B}_{s,e}^{-1}\cdot\boldsymbol{B}_{s,e})/\partial\boldsymbol{B}_{s,e} = \partial\boldsymbol{I}_s/\partial\boldsymbol{B}_{s,e} = \boldsymbol{0}$. The latter is valid since $\boldsymbol{B}_{s,e}$ is a tensor tangential to the interface in the current configuration, see Eqs. (25)–(26) and (45).

i.e., only the second term in the stress Eq. (57) enters in this condition, see Appendix B.6.

The fully-coupled closed set of equations for the generalised interfacial Maxwell model now reads (see Eqs. (31), (46), (55)–(56) and (59))

$$\begin{cases} \dot{\boldsymbol{B}}_{\mathrm{s,e}} = (\boldsymbol{L}_{\mathrm{s}} - \boldsymbol{D}_{\mathrm{s,p}}) \cdot \boldsymbol{B}_{\mathrm{s,e}} + \boldsymbol{B}_{\mathrm{s,e}} \cdot (\boldsymbol{L}_{\mathrm{s}} - \boldsymbol{D}_{\mathrm{s,p}})^{\mathrm{T}}, \\ \dfrac{\dot{J}_{\mathrm{s}}}{J_{\mathrm{s}}} = \mathrm{tr}(\boldsymbol{D}_{\mathrm{s}}), \\ \boldsymbol{D}_{\mathrm{s,p}} = \boldsymbol{D}^{\mathrm{h}}_{\mathrm{s,p}} + \boldsymbol{D}^{\mathrm{d}}_{\mathrm{s,p}}; \quad \boldsymbol{D}^{\mathrm{h}}_{\mathrm{s,p}} = \dfrac{1}{2\lambda_{\mathrm{D}}(J_1, J_2, J_{\mathrm{s}})} \boldsymbol{I}_{\mathrm{s}}, \\ \boldsymbol{D}^{\mathrm{d}}_{\mathrm{s,p}} = \dfrac{1}{2\lambda_{\mathrm{S}}(J_1, J_2, J_{\mathrm{s}})} \bar{\boldsymbol{B}}^{\mathrm{d}}_{\mathrm{s,e}}, \\ \boldsymbol{\tau}_{\mathrm{s}} = a_{\mathrm{D}}(J_1, J_2, J_{\mathrm{s}}) \boldsymbol{I}_{\mathrm{s}} + a_{\mathrm{S}}(J_1, J_2, J_{\mathrm{s}}) \bar{\boldsymbol{B}}^{\mathrm{d}}_{\mathrm{s,e}}, \end{cases} \tag{61}$$

where the stress tensor is related to the Helmholtz free energy per unit area, as shown by the first relation in Eq. (59). In the next sections, specific constitutive equations for $\boldsymbol{D}_{\mathrm{s,p}}$ and $\boldsymbol{\tau}_{\mathrm{s}}$ are suggested. Note, that the relative change in interfacial surface area J_{s} must in general be included as an additional independent variable, and that for thermodynamic admissibility also the condition in Eq. (60) must be fulfilled (see Appendix B.6). As explained in this section, in the following we will restrict our attention to models for which $\boldsymbol{\tau}_{\mathrm{s}} = \boldsymbol{\tau}_{\mathrm{s,c}}$.

3.3. Viscoelastic models

In this section, interfacial equivalents of some well-known non-linear viscoelastic bulk fluid models, namely the Upper-Convected Maxwell (UCM), Lower-Convected Maxwell (LCM) and Giesekus models, are presented. The interfacial UCM and LCM models are quasi-linear viscoelastic models, which we express in a Lodge-type integral for $\boldsymbol{\tau}_{\mathrm{s}}$, with an integrand consisting of an exponential memory function to account for stress relaxation using a single relaxation time, multiplied by finite interfacial strain tensors, such as $\boldsymbol{B}_{\mathrm{s}}$, and summed (integrated) over all past times. For the interfacial UCM and LCM models, in contrast to Eq. (61), we start by expressing the interfacial stress tensor $\boldsymbol{\tau}_{\mathrm{s}}$ in terms of the total interfacial Finger tensor $\boldsymbol{B}_{\mathrm{s}}$ and rate-of-deformation tensor $\boldsymbol{D}_{\mathrm{s}}$, rather than their elastic and plastic parts $\boldsymbol{B}_{\mathrm{s,e}}$ and $\boldsymbol{D}_{\mathrm{s,p}}$, respectively. Only after that, the connection with our framework of non-linear viscoelastic interface models, given by Eq. (61), will be made by specifying $\boldsymbol{D}_{\mathrm{s,p}}$ and $\boldsymbol{\tau}_{\mathrm{s}}$ in terms of $\boldsymbol{B}_{\mathrm{s,e}}$.

3.3.1. Upper-Convected Maxwell

To derive an interfacial equivalent of the Upper-Convected Maxwell (UCM) differential model for bulk fluids, we start from the Lodge model for interfaces given by (see [39])

$$\boldsymbol{\tau}_{\mathrm{s}} = \int_{-\infty}^{t} \frac{G}{\lambda} \exp\left(-\frac{t-t'}{\lambda}\right) (\boldsymbol{B}_{\mathrm{s}} - \boldsymbol{I}_{\mathrm{s}})\, dt', \tag{62}$$

where $\boldsymbol{\tau}_{\mathrm{s}}$ is the extra interfacial stress tensor, G and λ are the constant interfacial shear modulus and relaxation time, respectively, and $\boldsymbol{B}_{\mathrm{s}}$ is the interfacial Finger tensor at current time t with respect to reference time t', see Eq. (21), and $\boldsymbol{I}_{\mathrm{s}}$ is a function of t. Using $\boldsymbol{B}_{\mathrm{s}} - \boldsymbol{I}_{\mathrm{s}}$ as the strain tensor in Eq. (62) ensures that $\boldsymbol{\tau}_{\mathrm{s}}$ is tangential to the interface at all times t, see Eqs. (11) and (21). Differentiating Eq. (62) with respect to time t using the Leibniz integral rule yields

$$\begin{aligned} \dot{\boldsymbol{\tau}}_{\mathrm{s}} &= \frac{G}{\lambda} \exp\left(-\frac{t-t'}{\lambda}\right) (\boldsymbol{B}_{\mathrm{s}} - \boldsymbol{I}_{\mathrm{s}}) \Big|_{t'=t} \\ &\quad + \int_{-\infty}^{t} \frac{\partial}{\partial t} \left(\frac{G}{\lambda} \exp\left(-\frac{t-t'}{\lambda}\right) (\boldsymbol{B}_{\mathrm{s}} - \boldsymbol{I}_{\mathrm{s}}) \right) dt' \\ &= -\frac{1}{\lambda} \boldsymbol{\tau}_{\mathrm{s}} + \int_{-\infty}^{t} \frac{G}{\lambda} \exp\left(-\frac{t-t'}{\lambda}\right) \frac{\partial}{\partial t} (\boldsymbol{B}_{\mathrm{s}} - \boldsymbol{I}_{\mathrm{s}}) dt' \\ &= -\frac{1}{\lambda} \boldsymbol{\tau}_{\mathrm{s}} + \boldsymbol{L}_{\mathrm{s}} \cdot \boldsymbol{\tau}_{\mathrm{s}} + \boldsymbol{\tau}_{\mathrm{s}} \cdot \boldsymbol{L}_{\mathrm{s}}^{\mathrm{T}} + 2G\boldsymbol{D}_{\mathrm{s}}, \end{aligned} \tag{63}$$

where we have used Eq. (21) and in the last step we have substituted Eqs. (33), (62) and (B.9). Eq. (63) can then also be written as (see Eq. (35))

$$\lambda \overset{\nabla}{\boldsymbol{\tau}}_{\mathrm{s}} + \boldsymbol{\tau}_{\mathrm{s}} = 2\eta \boldsymbol{D}_{\mathrm{s}}, \tag{64}$$

with $\eta = G\lambda$ the interfacial shear viscosity.

The interfacial UCM model can also be expressed in terms of a differential equation for the interfacial conformation tensor $\boldsymbol{c}_{\mathrm{s}}$, which is defined by $\boldsymbol{\tau}_{\mathrm{s}} = G(\boldsymbol{c}_{\mathrm{s}} - \boldsymbol{I}_{\mathrm{s}})$. The evolution equation for $\boldsymbol{c}_{\mathrm{s}}$ is obtained by substituting $\boldsymbol{\tau}_{\mathrm{s}} = G(\boldsymbol{c}_{\mathrm{s}} - \boldsymbol{I}_{\mathrm{s}})$ into Eq. (64) using Eq. (36), which yields

$$\overset{\nabla}{\boldsymbol{c}}_{\mathrm{s}} = -\frac{1}{\lambda} (\boldsymbol{c}_{\mathrm{s}} - \boldsymbol{I}_{\mathrm{s}}). \tag{65}$$

Note that the evolution of $\boldsymbol{c}_{\mathrm{s}}$ is identical to that of $\boldsymbol{B}_{\mathrm{s,e}}$ if $\boldsymbol{D}_{\mathrm{s,p}} = 1/(2\lambda)(\boldsymbol{I}_{\mathrm{s}} - \boldsymbol{B}^{-1}_{\mathrm{s,e}})$: Eq. (65) is equivalent to Eqs. (47) and (55)–(56) if $1/\lambda_{\mathrm{D}} = (2J_2 - J_1)/(2\lambda J_2)$ and $1/\lambda_{\mathrm{S}} = 1/(\lambda J_{\mathrm{s,e}})$ (see Eq. (53)), which can be shown using Eq. (54). The expression for $\boldsymbol{\tau}_{\mathrm{s}}$ is obtained by using the interfacial Helmholtz free energy density per unit area in the current configuration $\psi_{\mathrm{s}} = (G/2)(J_1(\boldsymbol{c}_{\mathrm{s}}) - \ln(J_2(\boldsymbol{c}_{\mathrm{s}})) - 2)$ and applying Eq. (58), using the chain rule for differentiation, $\partial(J_1(\boldsymbol{c}_{\mathrm{s}}))/\partial \boldsymbol{c}_{\mathrm{s}} = \boldsymbol{I}_{\mathrm{s}}$ and $\partial(J_2(\boldsymbol{c}_{\mathrm{s}}))/\partial \boldsymbol{c}_{\mathrm{s}} = J_2(\boldsymbol{c}_{\mathrm{s}})\boldsymbol{c}_{\mathrm{s}}^{-1}$, and Eqs. (53)–(54); in accordance with the comment further above, it is assumed that $G \propto 1/J_{\mathrm{s}}$. For the rate of entropy production, or mechanical dissipation, to be non-negative for the interfacial UCM model, one must have (see Eq. (60)) $\boldsymbol{\tau}_{\mathrm{s}} : \boldsymbol{D}_{\mathrm{s,p}} = G/(2\lambda)(J_1(\boldsymbol{c}_{\mathrm{s}}) + J_1(\boldsymbol{c}_{\mathrm{s}}^{-1}) - 4) \geq 0$, which indeed holds for any $\boldsymbol{c}_{\mathrm{s}}$, as shown for the bulk UCM model [28]. This proves the thermodynamic consistency of the interfacial UCM model. Note that the expressions in this paragraph are the interfacial equivalents of those for the bulk UCM model, see [28].

3.3.2. Lower-Convected Maxwell

The interfacial differential Lower-Convected Maxwell (LCM) model can, in analogy to bulk, be derived from its integral form by replacing $\boldsymbol{B}_{\mathrm{s}} - \boldsymbol{I}_{\mathrm{s}}$ in the interfacial Lodge model from Eq. (62) by another interfacial strain tensor: $\boldsymbol{I}_{\mathrm{s}} - \boldsymbol{B}_{\mathrm{s}}^{-1}$. This results in [39]

$$\boldsymbol{\tau}_{\mathrm{s}} = \int_{-\infty}^{t} \frac{G}{\lambda} \exp\left(-\frac{t-t'}{\lambda}\right) (\boldsymbol{I}_{\mathrm{s}} - \boldsymbol{B}_{\mathrm{s}}^{-1})\, dt', \tag{66}$$

where $\boldsymbol{B}_{\mathrm{s}}^{-1}$ is the inverse of the interfacial Finger tensor at current time t with respect to reference time t', see Eq. (24), and $\boldsymbol{I}_{\mathrm{s}}$ is a function of t. Note that $\boldsymbol{B}_{\mathrm{s}}^{-1}$ is tangential to the interface, see Eq. (24). Taking the derivative of Eq. (66) with respect to t yields

$$\begin{aligned} \dot{\boldsymbol{\tau}}_{\mathrm{s}} &= \frac{G}{\lambda} \exp\left(-\frac{t-t'}{\lambda}\right) (\boldsymbol{I}_{\mathrm{s}} - \boldsymbol{B}_{\mathrm{s}}^{-1}) \Big|_{t'=t} \\ &\quad + \int_{-\infty}^{t} \frac{\partial}{\partial t} \left(\frac{G}{\lambda} \exp\left(-\frac{t-t'}{\lambda}\right) (\boldsymbol{I}_{\mathrm{s}} - \boldsymbol{B}_{\mathrm{s}}^{-1}) \right) dt' \\ &= -\frac{1}{\lambda} \boldsymbol{\tau}_{\mathrm{s}} + \int_{-\infty}^{t} \frac{G}{\lambda} \exp\left(-\frac{t-t'}{\lambda}\right) \frac{\partial}{\partial t} (\boldsymbol{I}_{\mathrm{s}} - \boldsymbol{B}_{\mathrm{s}}^{-1}) dt' \\ &= -\frac{1}{\lambda} \boldsymbol{\tau}_{\mathrm{s}} - (2\boldsymbol{D}_{\mathrm{s}} - \boldsymbol{L}_{\mathrm{s}}) \cdot \boldsymbol{\tau}_{\mathrm{s}} - \boldsymbol{\tau}_{\mathrm{s}} \cdot (2\boldsymbol{D}_{\mathrm{s}} - \boldsymbol{L}_{\mathrm{s}}^{\mathrm{T}}) + 2G\boldsymbol{D}_{\mathrm{s}}, \end{aligned} \tag{67}$$

where we have used Eqs. (21) and (24) and in the final step we have substituted Eqs. (38) and (B.9). Now, Eq. (67) can also be written as (see Eq. (40))

$$\lambda \overset{\Delta}{\boldsymbol{\tau}}_{\mathrm{s}} + \boldsymbol{\tau}_{\mathrm{s}} = 2\eta \boldsymbol{D}_{\mathrm{s}}, \tag{68}$$

showing, together with Eq. (64), that we can obtain objective constitutive equations for interfaces by using objective time derivatives in the differential equation and finite strain tensors in the integral equation.

The interfacial LCM model can also be expressed in terms of a differential equation for the inverse of the interfacial conformation tensor, $\boldsymbol{c}_{\mathrm{s}}^{-1}$, which is defined by $\boldsymbol{\tau}_{\mathrm{s}} = G(\boldsymbol{I}_{\mathrm{s}} - \boldsymbol{c}_{\mathrm{s}}^{-1})$. The evolution equation for $\boldsymbol{c}_{\mathrm{s}}^{-1}$ is obtained by substituting $\boldsymbol{\tau}_{\mathrm{s}} = G(\boldsymbol{I}_{\mathrm{s}} - \boldsymbol{c}_{\mathrm{s}}^{-1})$ into Eq. (68) using Eq. (41), giving

$$(\boldsymbol{c}_{\mathrm{s}}^{-1})^{\Delta} = \frac{1}{\lambda} (\boldsymbol{I}_{\mathrm{s}} - \boldsymbol{c}_{\mathrm{s}}^{-1}). \tag{69}$$

Note that the evolution of $\boldsymbol{c}_s^{-1}$ is identical to that of $\boldsymbol{B}_{s,e}^{-1}$ if $\boldsymbol{D}_{s,p} = 1/(2\lambda)(\boldsymbol{B}_{s,e} - \boldsymbol{I}_s)$: Eq. (69) is equivalent to Eqs. (50) and (55)–(56) if $1/\lambda_D = (J_1 - 2)/2\lambda$ and $1/\lambda_S = J_{s,e}/\lambda$ (see Eq. (53)), which can be shown using Eq. (54). The expression for $\boldsymbol{\tau}_s$ is obtained using the interfacial Helmholtz free energy density per unit area in the current configuration $\psi_s = G/2(J_1(\boldsymbol{c}_s^{-1}) - \ln(J_2(\boldsymbol{c}_s^{-1})) - 2)$ and by applying Eq. (58), using the chain rule for differentiation, $\partial(J_1(\boldsymbol{c}_s^{-1}))/\partial\boldsymbol{c}_s^{-1} = \boldsymbol{I}_s$ and $\partial(J_2(\boldsymbol{c}_s^{-1}))/\partial\boldsymbol{c}_s^{-1} = J_2(\boldsymbol{c}_s^{-1})\boldsymbol{c}_s$, and Eqs. (53)–(54); in accordance with the comment further above, it is assumed that $G \propto 1/J_s$. For the rate of entropy production, or mechanical dissipation, to be non-negative for the interfacial LCM model, one must have (see Eq. (60)) $\boldsymbol{\tau}_s : \boldsymbol{D}_{s,p} = G/(2\lambda)(J_1(\boldsymbol{c}_s) + J_1(\boldsymbol{c}_s^{-1}) - 4) \geq 0$, which indeed holds for any $\boldsymbol{c}_s^{-1}$, as shown for the interfacial UCM model in Section 3.3.1. This proves the thermodynamic consistency of the interfacial LCM model. Note that the expressions in this paragraph are the interfacial equivalents of those for the bulk LCM model, see [40].

3.3.3. Surface upper-convected Maxwell model from the literature

In addition to the interfacial UCM and LCM models presented in Sections 3.3.1–3.3.2, we have also tried to derive the surface upper-convected Maxwell (SUCM) model often encountered in the literature, see [11,15], starting from a similar Lodge-type integral as for UCM and LCM. The SUCM model is often written as two separate differential equations for the isotropic and deviatoric parts of the interfacial stress, with separate relaxation times and viscosities for dilatational and shear, respectively. As an effort to derive a single differential equation for the total interfacial stress tensor starting from a Lodge-type integral, we write

$$\boldsymbol{\tau}_s = \int_{-\infty}^{t} [c_D(t',t)(\mathrm{tr}(\boldsymbol{B}_s)/2)\boldsymbol{I}_s + c_S(t',t)\boldsymbol{B}_s^d]dt', \tag{70}$$

where $c_D(t',t)$ and $c_S(t',t)$ are memory functions for dilatation and shear, respectively. However, we were unfortunately not able to differentiate Eq. (70) with respect to time t and rewrite the result as a differential equation with isotropic and deviatoric parts of $\boldsymbol{\tau}_s$. This formulation of the SUCM model is often presented in the literature, see [11,15].

3.3.4. Giesekus model

The interfacial Giesekus model in the conformation-tensor formulation, with the interfacial conformation tensor defined by $\boldsymbol{\tau}_s = G(\boldsymbol{c}_s - \boldsymbol{I}_s)$, is written down by adding a quadratic term to account for anisotropic mobility to Eq. (65) for the interfacial UCM model. The evolution equation for $\boldsymbol{c}_s$ then becomes (see [28])

$$\lambda\overset{\nabla}{\boldsymbol{c}}_s + (\boldsymbol{c}_s - \boldsymbol{I}_s) + \alpha(\boldsymbol{c}_s - \boldsymbol{I}_s)^2 = \boldsymbol{0}, \tag{71}$$

with α a parameter that determines the magnitude of the anisotropic drag. It can be shown that the evolution of $\boldsymbol{c}_s$ in Eq. (71) is equivalent to that of $\boldsymbol{B}_{s,e}$ if $\boldsymbol{D}_{s,p} = 1/(2\lambda)(\alpha\boldsymbol{B}_{s,e} + (1-2\alpha)\boldsymbol{I}_s - (1-\alpha)\boldsymbol{B}_{s,e}^{-1})$: Eq. (71) is equivalent to Eqs. (47) and (55)–(56) if $1/\lambda_D = [-(1-\alpha)J_1/(2J_2) + (\alpha/2)J_1 + (1-2\alpha)]/\lambda$ and $1/\lambda_S = J_{s,e}[(1-\alpha)/J_2 + \alpha]/\lambda$ (see Eq. (53)), which can be shown using Eq. (54). The stress-tensor expression for the interfacial Giesekus model is the same as that for the interfacial UCM model, since the expression for the Helmholtz free energy area density ψ_s is the same for these models, see Section 3.3.1. For the rate of entropy production, or mechanical dissipation, to be non-negative for the Giesekus model, one must have (see Eq. (60)) $\boldsymbol{\tau}_s : \boldsymbol{D}_{s,p} = G/(2\lambda)[(1-\alpha)(J_1(\boldsymbol{c}_s) + J_1(\boldsymbol{c}_s^{-1}) - 4) + \alpha(\boldsymbol{c}_s : \boldsymbol{c}_s - 2J_1(\boldsymbol{c}_s) + 2)] \geq 0$ for $0 \leq \alpha < 1$, which indeed holds for any $\boldsymbol{c}_s$, as already shown for the bulk Giesekus model [28]. This proves the thermodynamic consistency of the interfacial Giesekus model. Note that the expressions in this paragraph are the interfacial equivalents of those for the bulk Giesekus model, see [28].

3.3.5. Summary

The interfacial upper- and lower-convected Maxwell (UCM and LCM) models are derived by expressing the interfacial stress tensor in a Lodge-type integral using finite strain tensors $\boldsymbol{B}_{s,e}$ and $\boldsymbol{B}_{s,e}^{-1}$, respectively. These models are re-formulated in terms of an interfacial conformation-tensor $\boldsymbol{c}_s$; by adding a term that is quadratic in the conformation tensor to the UCM equation, the interfacial Giesekus model is obtained. These models can also be derived from their corresponding interfacial Helmholtz free energy area density in terms of $\boldsymbol{c}_s$ (or its inverse in case of the LCM model), have a non-negative entropy-production rate for relevant choices of material parameters, and furthermore fit into our framework for non-linear viscoelastic interface models. Note, that the models discussed in this section do not have separate material parameters for dilatation and shear with separate equations for the isotropic and deviatoric parts of the stress tensor. This is in contrast with the surface UCM model often encountered in the literature, which we were unfortunately not able to write in the form of a Lodge-type integral for the total stress tensor.

4. Elastoviscoplastic interface model

Our framework for non-linear viscoelastic interfaces described in Eq. (61) is used to model elastoviscoplastic behaviour of interfaces as explained in Section 3. A specific constitutive equation for the interfacial stress tensor $\boldsymbol{\tau}_s$ and for the plastic surface rate-of-deformation tensor $\boldsymbol{D}_{s,p}$ is chosen. This choice describes a generalised interfacial Maxwell model with relaxation speeds for shear and dilatation that depend on stress. For this non-linear viscoelastic model, the elastic stress in the spring equals the viscous stress in the dashpot, see the mechanical representation of the Maxwell element in Fig. 3. Hence, plastic deformation (of the dashpot) is driven by interfacial stress (in the spring). The viscoelastic interfacial stress in the Maxwell element is obtained from the Helmholtz free energy area density based on the Hütter–Tervoort model for hyperelastic solid interfaces [13,14]. As theirs is a hyperelastic interface model while we aim at modelling interfacial elastoviscoplasticity, we choose the interfacial Helmholtz free energy density per unit area in the reference configuration, $\hat{\psi}_s$, as follows:

$$\hat{\psi}_s = \frac{K}{2}(\ln(J_{s,e}))^2 + \frac{G}{2}\mathrm{tr}(\bar{\boldsymbol{B}}_{s,e} - \boldsymbol{I}_s), \tag{72}$$

where K and G are the interfacial dilatational and shear moduli, respectively, with $K \geq 0$ and $G \geq 0$. This expression for $\hat{\psi}_s$ is obtained from the one in Pepicelli et al. [14] by replacing $\boldsymbol{B}_s$ with $\boldsymbol{B}_{s,e}$. The interfacial stress $\boldsymbol{\tau}_s$ can then be derived using Eq. (58), the chain rule for differentiation, $\partial J_1/\partial\boldsymbol{B}_{s,e} = \boldsymbol{I}_s$ and $\partial J_2/\partial\boldsymbol{B}_{s,e} = J_2\boldsymbol{B}_{s,e}^{-1}$, and Eqs. (53)–(54), giving

$$\boldsymbol{\tau}_s = \frac{K\ln(J_{s,e})}{J_s}\boldsymbol{I}_s + \frac{G}{J_s}\bar{\boldsymbol{B}}_{s,e}^d. \tag{73}$$

Other choices for $\hat{\psi}_s$, and hence for $\boldsymbol{\tau}_s$, could also have been made. An argument in favour of Eq. (73) is the following: Using $\boldsymbol{B}_{s,e}$ instead of $\boldsymbol{B}_s$ in $\hat{\psi}_s$ means that there is no permanent network, and all of the microstructure can relax (e.g. independent polymer coils that can be distorted individually, but these coils are not connected to form a network). Therefore, if such a system is continuously dilated, the distortion of such individual elastic coils remains finite while at the same time their area density decreases, and therefore the stress decreases. This "dilution" effect is accounted for by the factor $1/J_s$.

For specifying $\boldsymbol{D}_{s,p}$ in Eq. (61), expressions for the relaxation speeds are given by

$$\frac{1}{\lambda_D} = \frac{1}{\lambda_{ref,D}}\frac{\ln(J_{s,e})}{J_s}\frac{\sinh(\tau_{eq,D}/\tau_{ref,D})}{\tau_{eq,D}/\tau_{ref,D}},$$
$$\frac{1}{\lambda_S} = \frac{1}{\lambda_{ref,S}}\frac{1}{J_s}\frac{\sinh(\tau_{eq,S}/\tau_{ref,S})}{\tau_{eq,S}/\tau_{ref,S}}, \tag{74}$$

which are based on an Eyring viscosity function [30–34] to account for the gradual but rather sharp transition from a predominantly elastic response at low stress levels to primarily viscous behaviour at high stress levels. A motivation for why these are called relaxation speeds for dilatation and shear, respectively, will be provided later in the paper. In Eq. (74), $1/\lambda_{\mathrm{ref,D}}$ and $1/\lambda_{\mathrm{ref,S}}$ are relaxation speed constants for interfacial dilatation and shear, respectively. The scalars $\tau_{\mathrm{eq,D}} = J_1(\boldsymbol{\tau}_{\mathrm{s}})/2 = \frac{1}{2}\mathrm{tr}(\boldsymbol{\tau}_{\mathrm{s}})$ and $\tau_{\mathrm{eq,S}} = \sqrt{-J_2(\boldsymbol{\tau}_{\mathrm{s}}^{\mathrm{d}})}$ are equivalent stress scalars, and $\tau_{\mathrm{ref,D}}$ and $\tau_{\mathrm{ref,S}}$ are material constants with the units of stress. It can be seen that for an interfacial stress tensor given by $\boldsymbol{\tau}_{\mathrm{s}} = \sigma(\boldsymbol{e}_{xx} + \boldsymbol{e}_{yy}) + \tau(\boldsymbol{e}_{xy} + \boldsymbol{e}_{yx})$, $\tau_{\mathrm{eq,D}} = \sigma$ and $\tau_{\mathrm{eq,S}} = \tau$. In particular, it can be shown for the representation in Eq. (73) that

$$\tau_{\mathrm{eq,D}} = \frac{K\ln(J_{\mathrm{s,e}})}{J_{\mathrm{s}}}, \qquad \tau_{\mathrm{eq,S}} = \frac{G}{J_{\mathrm{s}}}\sqrt{-J_2(\bar{\boldsymbol{B}}_{\mathrm{s,e}}^{\mathrm{d}})}. \tag{75}$$

The rate of interfacial entropy-production, or the mechanical dissipation, for the elastoviscoplastic interface model is non-negative since $\boldsymbol{\tau}_{\mathrm{s}} : \boldsymbol{D}_{\mathrm{s,p}} = (K/\lambda_{\mathrm{ref,D}})(\ln(J_{\mathrm{s,e}})/J_{\mathrm{s}})^2 \sinh(\tau_{\mathrm{eq,D}}/\tau_{\mathrm{ref,D}})/(\tau_{\mathrm{eq,D}}/\tau_{\mathrm{ref,D}}) + \frac{1}{2}(G/\lambda_{\mathrm{ref,S}})(1/J_{\mathrm{s}})^2 \sinh(\tau_{\mathrm{eq,S}}/\tau_{\mathrm{ref,S}})/(\tau_{\mathrm{eq,S}}/\tau_{\mathrm{ref,S}})(\bar{\boldsymbol{B}}_{\mathrm{s,e}}^{\mathrm{d}} : \bar{\boldsymbol{B}}_{\mathrm{s,e}}^{\mathrm{d}}) \geq 0$ (see Eqs. (60)–(61) and (73)–(74)). This shows that the specific choices for $\boldsymbol{\tau}_{\mathrm{s}}$, $1/\lambda_{\mathrm{D}}$ and $1/\lambda_{\mathrm{S}}$ of Eqs. (73) and (74) guarantee thermodynamic admissibility if both $1/\lambda_{\mathrm{ref,D}} \geq 0$ and $1/\lambda_{\mathrm{ref,S}} \geq 0$. In the next section, the elastoviscoplastic model for interfaces in Eqs. (61) and (73)–(74) will be evaluated for interfacial dilatational and shear flow.

In summary, the equations for our elastoviscoplastic interface model showing a clear separation between dilatation and shear, become (see also the more general Eq. (61))

$$\begin{cases} \dot{\boldsymbol{B}}_{\mathrm{s,e}} = (\boldsymbol{L}_{\mathrm{s}} - \boldsymbol{D}_{\mathrm{s,p}}) \cdot \boldsymbol{B}_{\mathrm{s,e}} + \boldsymbol{B}_{\mathrm{s,e}} \cdot (\boldsymbol{L}_{\mathrm{s}} - \boldsymbol{D}_{\mathrm{s,p}})^{\mathrm{T}}, \\ \dfrac{\dot{J}_{\mathrm{s}}}{J_{\mathrm{s}}} = \mathrm{tr}(\boldsymbol{D}_{\mathrm{s}}), \\ \boldsymbol{D}_{\mathrm{s,p}} = \dfrac{1}{2\lambda_{\mathrm{ref,D}}} \dfrac{\ln(J_{\mathrm{s,e}})}{J_{\mathrm{s}}} \dfrac{\sinh(\tau_{\mathrm{eq,D}}/\tau_{\mathrm{ref,D}})}{\tau_{\mathrm{eq,D}}/\tau_{\mathrm{ref,D}}} \boldsymbol{I}_{\mathrm{s}} \\ \qquad + \dfrac{1}{2\lambda_{\mathrm{ref,S}}} \dfrac{1}{J_{\mathrm{s}}} \dfrac{\sinh(\tau_{\mathrm{eq,S}}/\tau_{\mathrm{ref,S}})}{\tau_{\mathrm{eq,S}}/\tau_{\mathrm{ref,S}}} \bar{\boldsymbol{B}}_{\mathrm{s,e}}^{\mathrm{d}}, \\ \boldsymbol{\tau}_{\mathrm{s}} = \dfrac{K\ln(J_{\mathrm{s,e}})}{J_{\mathrm{s}}} \boldsymbol{I}_{\mathrm{s}} + \dfrac{G}{J_{\mathrm{s}}} \bar{\boldsymbol{B}}_{\mathrm{s,e}}^{\mathrm{d}}. \end{cases} \tag{76}$$

The interfacial stress tensor $\boldsymbol{\tau}_{\mathrm{s}}$ is derived from the expression for the interfacial Helmholtz free energy area density for a hyperelastic interface, by replacing in that expression the interfacial Finger tensor with its elastic part $\boldsymbol{B}_{\mathrm{s,e}}$. Thermodynamic consistency is guaranteed for relaxation time constants that satisfy $1/\lambda_{\mathrm{ref,D}} \geq 0$ and $1/\lambda_{\mathrm{ref,S}} \geq 0$, see the text below Eq. (75).

5. Application to homogeneous flows

In order to examine whether our elastoviscoplastic model for interfaces qualitatively describes the behaviour observed in the experimental literature, see Section 1, model predictions have been examined numerically. For this purpose, Eq. (76) is applied to the cases of the homogeneous interfacial simple shear and dilatational flows. The equations are integrated in time using a second-order explicit Runge–Kutta time-discretisation scheme (Heun's method) [41] using a time step of $10^{-4}\lambda_{\mathrm{ref,S}}$ for shear and $10^{-4}\lambda_{\mathrm{ref,D}}$ for dilatation. The initial condition $\boldsymbol{B}_{\mathrm{s,e}}(t=0) = \boldsymbol{I}_{\mathrm{s,0}}$ is used. Results of single-point calculations are presented and discussed in the next sections.

5.1. Single-point calculations for simple shear

Focussing on shear first, the surface velocity gradient tensor for this homogeneous flow is given by $\boldsymbol{L}_{\mathrm{s}} = \dot{\gamma}\boldsymbol{e}_x\boldsymbol{e}_y$, with $\dot{\gamma}$ the constant shear rate and where $\boldsymbol{e}_x$ is the velocity direction and $\boldsymbol{e}_y$ is the gradient direction, both tangential to the flat interface. Therefore, $\dot{J}_{\mathrm{s}} = 0$ since $\mathrm{tr}(\boldsymbol{D}_{\mathrm{s}}) = 0$ (see Eq. (31)), and $J_{\mathrm{s}} = 1$ for all times t, by virtue of the initial condition $J_{\mathrm{s}}(t=0) = 1$. Furthermore, it can be shown on the basis of the dynamics of $J_{\mathrm{s,e}}$ (see Eqs. (44), (55)–(56) and (74)) that $\dot{J}_{\mathrm{s,e}}/J_{\mathrm{s,e}} = (\ln(J_{\mathrm{s,e}}))^{\cdot} = -1/\lambda_{\mathrm{D}} \propto -\ln(J_{\mathrm{s,e}})$, which represents relaxation towards $\ln(J_{\mathrm{s,e}}) = 0$, i.e., towards $J_{\mathrm{s,e}} = 1$; therefore, if one starts with $\boldsymbol{B}_{\mathrm{s,e}}(t=0) = \boldsymbol{I}_{\mathrm{s}}$, one will have $J_{\mathrm{s,e}} = 1$ for all times. As a consequence, $\boldsymbol{\tau}_{\mathrm{s}} = \boldsymbol{\tau}_{\mathrm{s}}^{\mathrm{d}}$ (see Eq. (73)), $1/\lambda_{\mathrm{D}} = 0$ (see Eq. (74)), $\boldsymbol{D}_{\mathrm{s,p}} = \boldsymbol{D}_{\mathrm{s,p}}^{\mathrm{d}}$ (see Eqs. (55)–(56)), and $J_{\mathrm{s,e}} = J_{\mathrm{s}} = 1$ if the initial condition is $\boldsymbol{B}_{\mathrm{s,e}}(t=0) = \boldsymbol{I}_{\mathrm{s}}$ (see Eq. (44)). The elastoviscoplastic model for interfaces applied to simple shear is then expressed as (see Eq. (76)):

$$\begin{cases} \dot{\boldsymbol{B}}_{\mathrm{s,e}} = (\boldsymbol{L}_{\mathrm{s}} - \boldsymbol{D}_{\mathrm{s,p}}) \cdot \boldsymbol{B}_{\mathrm{s,e}} + \boldsymbol{B}_{\mathrm{s,e}} \cdot (\boldsymbol{L}_{\mathrm{s}} - \boldsymbol{D}_{\mathrm{s,p}})^{\mathrm{T}}, \\ \boldsymbol{D}_{\mathrm{s,p}} = \dfrac{1}{2\lambda_{\mathrm{ref,S}}} \dfrac{\sinh(\tau_{\mathrm{eq,S}}/\tau_{\mathrm{ref,S}})}{\tau_{\mathrm{eq,S}}/\tau_{\mathrm{ref,S}}} \boldsymbol{B}_{\mathrm{s,e}}^{\mathrm{d}}, \\ \boldsymbol{\tau}_{\mathrm{s}} = G\boldsymbol{B}_{\mathrm{s,e}}^{\mathrm{d}}, \quad \tau_{\mathrm{eq,S}} = G\sqrt{-J_2(\boldsymbol{B}_{\mathrm{s,e}}^{\mathrm{d}})}. \end{cases} \tag{77}$$

By substituting $\boldsymbol{D}_{\mathrm{s,p}}$ and $1/\lambda_{\mathrm{S}}$ into the equation for $\dot{\boldsymbol{B}}_{\mathrm{s,e}}$, it can be easily seen why $1/\lambda_{\mathrm{S}}$ ($1/\lambda_{\mathrm{ref,S}}$) is called the relaxation speed for shear (at zero stress).

Making the equation for $\dot{\boldsymbol{B}}_{\mathrm{s,e}}$ in Eq. (77) dimensionless by scaling time with $1/\dot{\gamma}$, it can be seen that there are two dimensionless groups: $\dot{\gamma}\lambda_{\mathrm{ref,S}}$ and $\tau_{\mathrm{ref,S}}/G$. These groups govern the entire evolution of $\boldsymbol{B}_{\mathrm{s,e}}$, or equivalently that of $\boldsymbol{\tau}_{\mathrm{s}}$, for this flow. Fig. 4 shows the shear stress τ as a function of the shear strain $\dot{\gamma}t$ for different values of $\dot{\gamma}\lambda_{\mathrm{ref,S}}$ and $\tau_{\mathrm{ref,S}}/G$. In Fig. 4a, $\tau_{\mathrm{ref,S}}/G = 1$ is chosen and $\dot{\gamma}\lambda_{\mathrm{ref,S}}$ is varied, while in Fig. 4b $\dot{\gamma}\lambda_{\mathrm{ref,S}} = 10$ is set and a range of $\tau_{\mathrm{ref,S}}/G$ values is chosen. An elastic response is observed at small $\dot{\gamma}t$, for which τ increases approximately linearly with $\dot{\gamma}t$. While τ is increasing, it is deviating more and more from the elastic behaviour as relaxation occurs and hence plastic flow sets in. An overshoot in τ follows for higher values of $\dot{\gamma}\lambda_{\mathrm{ref,S}}$ and $\tau_{\mathrm{ref,S}}/G$; the lower the values of the dimensionless numbers, the smaller the overshoot. Eventually, τ reaches a steady-state value. This linear-elastic regime at smaller stresses with a transition at higher stresses towards a plastic plateau directly or via strain softening, is in qualitative agreement with interfacial shear rheometry results from the literature, see e.g. [2–4]. The overshoot and subsequent strain softening of the shear stress τ in Fig. 4 are related to the tensorial structure of Eq. (77) as a result of our choice for $\boldsymbol{D}_{\mathrm{s,p}}$. For the overshoot to occur it is required (though not sufficient) that the non-shear components of $\boldsymbol{\tau}_{\mathrm{s}}$, or equivalently those of $\boldsymbol{B}_{\mathrm{s,e}}$, are still evolving while for the shear stress $\dot{\tau} = 0$ at the maximum in τ, see Eq. (77). The values of the shear stress τ_{os} and the shear strain γ_{os} at the overshoot are plotted as functions of a wide range of both $\dot{\gamma}\lambda_{\mathrm{ref,S}}$ and $\tau_{\mathrm{ref,S}}/G$ in Fig. 5. In addition, Fig. 6 plots the relative strength of the overshoot $(\tau_{\mathrm{os}} - \tau_{\infty})/\tau_{\infty}$, with τ_{∞} the steady-state value of τ, versus $\dot{\gamma}\lambda_{\mathrm{ref,S}}$ and $\tau_{\mathrm{ref,S}}/G$. In both Figs. 5–6, for the given ranges of $\dot{\gamma}\lambda_{\mathrm{ref,S}}$ and $\tau_{\mathrm{ref,S}}/G$, only the region is plotted for which $(\tau_{\mathrm{os}} - \tau_{\infty})/\tau_{\infty} \geq 10^{-3}$ holds true. This region has been projected onto the $\tau_{\mathrm{os}} = \gamma_{\mathrm{os}} = 0$ planes of Fig. 5, indicated by the black-shaded areas. The dependence of τ_{os}, γ_{os} and $(\tau_{\mathrm{os}} - \tau_{\infty})/\tau_{\infty}$ on $\dot{\gamma}\lambda_{\mathrm{ref,S}}$ and $\tau_{\mathrm{ref,S}}/G$ shown in Figs. 5–6 is highly non linear, which becomes more pronounced at higher values of $\tau_{\mathrm{ref,S}}/G$ and $\dot{\gamma}\lambda_{\mathrm{ref,S}}$, respectively. It can also be seen in the same figures that $\tau_{\mathrm{os}} \to 0$, $\gamma_{\mathrm{os}} \to 0$ and $(\tau_{\mathrm{os}} - \tau_{\infty})/\tau_{\infty} \to 0$ if $\tau_{\mathrm{ref,S}}/G \to 0$, which means that the overshoot occurs at smaller values of the shear strain $\dot{\gamma}t$ and becomes less significant as $\tau_{\mathrm{ref,S}}/G$ is decreased (see also Fig. 4b).

5.2. Single-point calculations for dilatation

For dilatation, the surface velocity gradient tensor is given by $\boldsymbol{L}_{\mathrm{s}} = (\dot{e}/2)(\boldsymbol{e}_x\boldsymbol{e}_x + \boldsymbol{e}_y\boldsymbol{e}_y)$, with constant dilatational rate $\dot{e}$ and where $\boldsymbol{e}_x$ and $\boldsymbol{e}_y$ are perpendicular directions in the plane of the flat interface. Because of isotropic deformation, the interfacial stress is isotropic and hence shear stresses are not present. This implies that $\bar{\boldsymbol{B}}_{\mathrm{s,e}}^{\mathrm{d}} = \boldsymbol{0}$ (see Eq. (73)) and therefore $\boldsymbol{D}_{\mathrm{s,p}} = \boldsymbol{D}_{\mathrm{s,p}}^{\mathrm{h}}$ (see Eqs. (55)–(56)). Then, the evolution of $\boldsymbol{B}_{\mathrm{s,e}}$ in Eq. (76) applied to dilatation reduces to Eq. (44) for the evolution of $J_{\mathrm{s,e}}$, since there is just interfacial surface area deformation. This gives

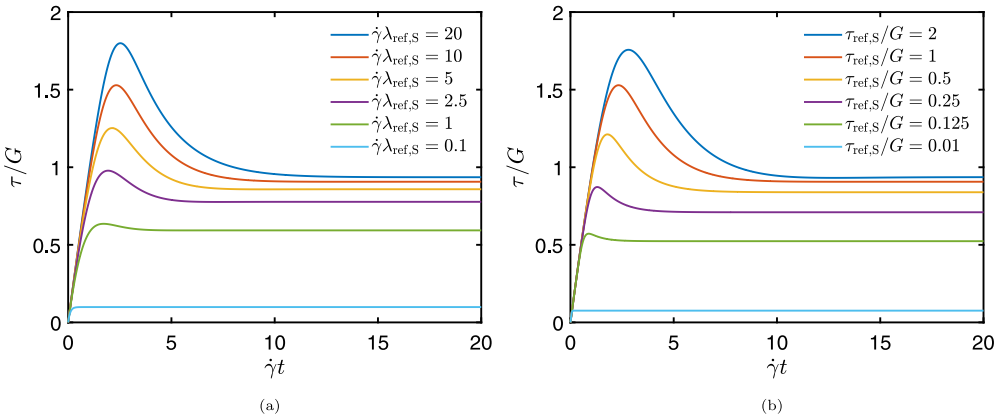

Fig. 4. Shear stress τ as a function of the shear strain $\dot{\gamma}t$ for $\tau_{\mathrm{ref,S}}/G = 1$ and different values of $\dot{\gamma}\lambda_{\mathrm{ref,S}}$ (a), and for $\dot{\gamma}\lambda_{\mathrm{ref,S}} = 10$ and different values of $\tau_{\mathrm{ref,S}}/G$ (b).

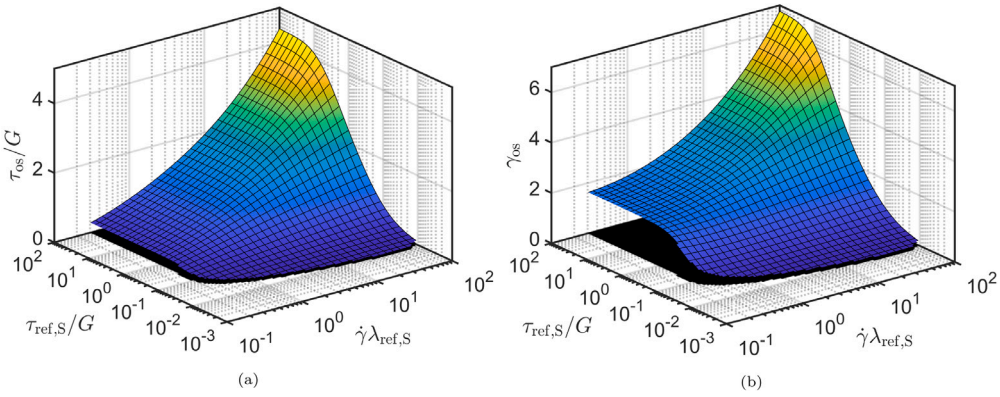

Fig. 5. Shear stress (a) and shear strain (b) at the overshoot as a function of the dimensionless numbers $\dot{\gamma}\lambda_{\mathrm{ref,S}}$ and $\tau_{\mathrm{ref,S}}/G$.

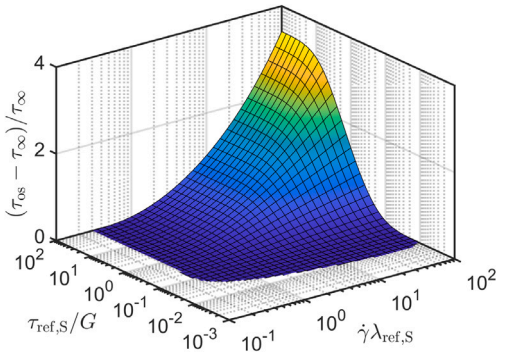

Fig. 6. Overshoot in shear stress relative to the steady-state shear stress for different values of the dimensionless numbers $\dot{\gamma}\lambda_{\mathrm{ref,S}}$ and $\tau_{\mathrm{ref,S}}/G$.

the following elastoviscoplastic interface model applied to dilatation (see Eq. (76)):

$$\begin{cases} \dfrac{\dot{J}_{\mathrm{s,e}}}{J_{\mathrm{s,e}}} = \mathrm{tr}(\boldsymbol{D}_{\mathrm{s}} - \boldsymbol{D}_{\mathrm{s,p}}), \\ \dfrac{\dot{J}_{\mathrm{s}}}{J_{\mathrm{s}}} = \mathrm{tr}(\boldsymbol{D}_{\mathrm{s}}), \\ \boldsymbol{D}_{\mathrm{s,p}} = \dfrac{1}{2\lambda_{\mathrm{ref,D}}} \dfrac{\ln(J_{\mathrm{s,e}})}{J_{\mathrm{s}}} \dfrac{\sinh(\tau_{\mathrm{eq,D}}/\tau_{\mathrm{ref,D}})}{\tau_{\mathrm{eq,D}}/\tau_{\mathrm{ref,D}}} \boldsymbol{I}_{\mathrm{s}}, \\ \boldsymbol{\tau}_{\mathrm{s}} = \dfrac{K \ln(J_{\mathrm{s,e}})}{J_{\mathrm{s}}} \boldsymbol{I}_{\mathrm{s}}, \quad \tau_{\mathrm{eq,D}} = \dfrac{K \ln(J_{\mathrm{s,e}})}{J_{\mathrm{s}}}. \end{cases} \tag{78}$$

By substituting $\boldsymbol{D}_{\mathrm{s,p}}$ and $1/\lambda_{\mathrm{D}}$ into $\dot{J}_{\mathrm{s,e}}/J_{\mathrm{s,e}}$ it can be seen why $1/\lambda_{\mathrm{D}}$ ($1/\lambda_{\mathrm{ref,D}}$) is called relaxation speed (constant) for dilatation. It is also observed that initially the response is purely elastic, i.e. $\boldsymbol{D}_{\mathrm{s,p}} = \boldsymbol{0}$ since $\ln(J_{\mathrm{s,e}}) = 0$ for the initial conditions $J_{\mathrm{s,e}}(t = 0) = J_{\mathrm{s}}(t = 0) = 1$.

Non-dimensionalising the equation for $\dot{J}_{\mathrm{s,e}}/J_{\mathrm{s,e}}$ in Eq. (78) by scaling time with $1/\dot{\epsilon}$, it can be seen that there are two dimensionless groups: $\dot{\epsilon}\lambda_{\mathrm{ref,D}}$ and $\tau_{\mathrm{ref,D}}/K$. However, the value of the dilatational rate $\dot{\epsilon}$ itself is also important as it governs the dynamics of J_{s} appearing in $\boldsymbol{D}_{\mathrm{s,p}}$ and $\boldsymbol{\tau}_{\mathrm{s}}$ (see Eq. (78)). These dimensionless groups and $\dot{\epsilon}$ govern the evolution of the interfacial dilatational stress $\sigma = K \ln(J_{\mathrm{s,e}})/J_{\mathrm{s}}$ (see Eq. (78)) for this flow. The evolution of σ as a function of the Hencky strain $\ln(J_{\mathrm{s}}) = \dot{\epsilon}t$ is plotted in Fig. 7a for $\tau_{\mathrm{ref,D}}/K = 1$ and three sets of values for $\dot{\epsilon}\lambda_{\mathrm{ref,D}}$, and in Fig. 7b for $\dot{\epsilon}\lambda_{\mathrm{ref,D}} = 0.2$ and three sets of values for $\tau_{\mathrm{ref,D}}/K$. The value of the relaxation-time constant is kept constant at $\lambda_{\mathrm{ref,D}} = 1$. Fig. 7a shows that at small $\dot{\epsilon}t$, σ increases linearly as a function of $\dot{\epsilon}t$; upon further deformation, the slope of σ gradually decreases and σ reaches a maximum. The larger the value of $\dot{\epsilon}\lambda_{\mathrm{ref,D}}$, the larger the linear regime (in terms of $\dot{\epsilon}t$), and the larger the stress and strain at the maximum. Upon even further deformation, σ decreases as a function of $\dot{\epsilon}t$. Fig. 7a shows that this decrease in σ beyond the maximum can be postponed (in terms of $\dot{\epsilon}t$) by decreasing $\tau_{\mathrm{ref,D}}/K$. Decreasing $\tau_{\mathrm{ref,D}}/K$ leads in turn to a lower stress and strain at the maximum.

6. Discussion: comparison with the Eindhoven Glassy Polymer model

The elastoviscoplastic interface model introduced in this paper can be considered as the interfacial equivalent of the Eindhoven Glassy Polymer (EGP) model [30–34]. The EGP model is a constitutive equation including yielding and the large-strain post-yield deformation of

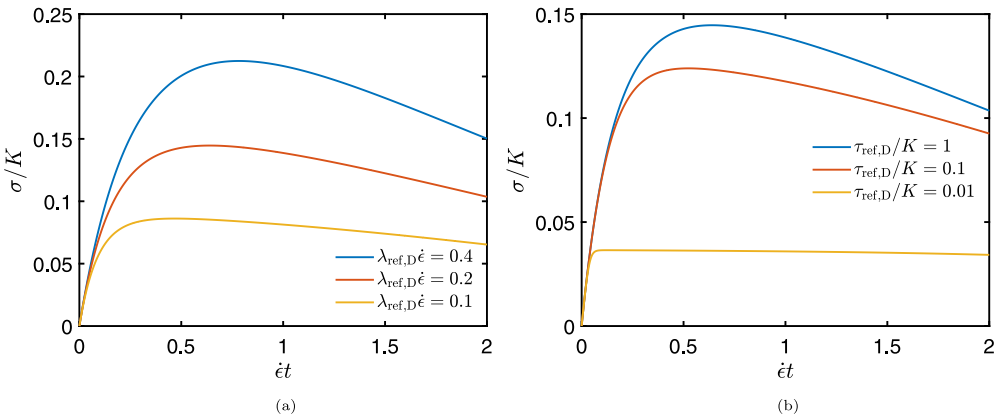

Fig. 7. Interfacial dilatational stress σ as a function of the Hencky strain $\ln(J_s) = \dot{\epsilon}t$ for $\tau_{\mathrm{ref,D}}/K = 1$ and different values of $\dot{\epsilon}\lambda_{\mathrm{ref,D}}$ (a), and for $\dot{\epsilon}\lambda_{\mathrm{ref,D}} = 0.2$ and different values of $\tau_{\mathrm{ref,D}}/K$ (b). The value of the relaxation-time constant is $\lambda_{\mathrm{ref,D}} = 1$.

glassy-polymer bulk materials. It is not a yield-surface model but it uses a strongly stress-dependent Eyring viscosity to mimic the transition from elastic to plastic behaviour. Plastic flow at yield is considered as stress-induced rearrangements of microscopic entities. The difference between our model and the EGP model is that our model describes deformation (rate) and stress of an interface material using interfacial tensors of rank two, compared to bulk tensors of rank three with the EGP model for a bulk material. Therefore, the tensors $\boldsymbol{B}_{\mathrm{s,e}}$ and $\boldsymbol{\tau}_{\mathrm{s}}$ in our model have no components in the direction perpendicular to the interface, generally in contrast with the bulk Finger and stress tensors in the 3D version of the EGP model. In addition, the 3D version of the EGP model assumes incompressible plastic flow so that the volume response is purely elastic, which is a valid assumption for bulk polymer glasses. In contrast, our model does take into account changes in the interface surface area due to plastic deformation, by choosing $\boldsymbol{D}^{\mathrm{h}}_{\mathrm{s,p}} \neq \boldsymbol{0}$, since for interfaces this has been shown to be important [5–7,12]. In comparing an interface model with a bulk model, furthermore note that volume (in)compressibility of material adjacent to the boundary does not imply that the boundary itself is (in)compressible. If one assumes plastic incompressibility of the interface ($J_{\mathrm{s}} = J_{\mathrm{s,e}}$), the structure of Eqs. (61) and (73)–(75) is very similar to that of the EGP model. Nevertheless, the predictions are different if the models are applied to the cases of simple shear and dilatation, for example, see Eqs. (77)–(78) and [30–34].

7. Conclusions and recommendations

A constitutive framework has been developed to model the non-linear viscoelastic behaviour of sharp interfaces, with applications to quasi-linear viscoelasticity and elastoviscoplasticity. For this purpose, the total deformation of the interface is multiplicatively split into an elastic and a plastic part. The framework has been formulated in terms of an evolution equation for the internal deformation variable, the elastic part of the interfacial Finger tensor, as a function of the external deformation-rate variable, the surface velocity gradient tensor. Constitutive equations have been provided for the plastic surface rate-of-deformation tensor and the extra interfacial stress tensor in terms of the elastic part of the interfacial Finger tensor and the relative change in interfacial area. This framework, with a proper description of interface kinematics and stress, is used for modelling isotropic elasto-viscoplasticity of interfaces, i.e. the interface shows behaviour between that of a fluid and a solid. The model has a clear separation between interfacial dilatation and shear, which is also useful for experiments. For this purpose, separate Eyring relaxation times for dilatation and shear that depend on stress are chosen to describe the relaxation of elastic deformation. The approach is similar to one that has already been successful in describing the mechanical behaviour of bulk polymer glasses. Our interface material model is a generalisation of the Eindhoven Glassy Polymer (EGP) model for bulk polymer glasses, by also taking into account the effect of plastic surface-area changes of the interface. The thermodynamic admissibility of our model has been proven by showing that the entropy-production rate is non-negative for non-negative relaxation time constants.

Applied to the case of simple shear flow, our elastoviscoplastic interface model has been shown to qualitatively describe the behaviour observed in the experimental literature, see e.g. [2–4]. These experiments involve standard interfacial rheometric tests at flat air–water and oil–water interfaces, which are typically covered with surface-active particles, asphaltene molecules, surfactant molecules, proteins, polymers and lipids. For qualitative agreement with experiments we refer to our model prediction of a primarily elastic response at small deformations, followed by a gradual but rather sharp transition to mainly plastic flow as the stress increases. By qualitative agreement we furthermore mean that at the yield point, the shear stress reaches a maximum; upon further deformation it decreases again until it finds a plateau. It has been shown how (the relative strength of) the shear stress and the shear strain at the overshoot are controlled by varying the dimensionless groups of parameters in the model. Furthermore, the model predicts a non-zero first normal-stress difference in shear (not shown in this paper). In interfacial dilatational flow, elastoviscoplastic behaviour with a stress maximum is predicted, followed by a decreasing stress without a plateau upon deformation beyond the strain at the stress maximum. The linear elastic regime, the stress and strain at the maximum, and the rate at which the stress decreases after the maximum, have been shown to be controlled by the parameters in the model.

If so desired, strain softening in dilatation can be finetuned by including a softening parameter in the Eyring relaxation-time functions (see [31–33] for the case of a 3D bulk description). Another extension to the model presented in this paper is incorporating post-yield strain hardening effects with a spring linked in parallel with the Maxwell element, by adding a Neo-Hookean hardening stress tensor to the interfacial stress [31–33]. An increase in interfacial shear stress after yielding has been observed for e.g. proteins at an air–water interface. This has been attributed to the build-up of a transient network during shearing [4]. Strain hardening has also been observed for polymer layers at an air–water interface in interfacial uniaxial extension [6], and in dilatation [7]. Developing interfacial rheometers that can measure first normal stress differences (which to the best of our knowledge are not yet discussed in the literature) would be useful for model selection. Further research steps include implementing this model framework in our validated in-house finite-element code [18] and applying this to a relevant complex flow problem to investigate the influence of interfacial rheology, e.g. interfacial plasticity, on the behaviour on larger scales.

Table A.1
List of interfacial tensors appearing in this paper, stating which of their two sides have out-of-plane directions with respect to the tangent space of the interface in the current configuration.

Name	Symbol	Out-of-plane directions in current configuration
Interfacial (extra) stress tensor	$\boldsymbol{\tau}_s$	No
Surface unit tensor	$\boldsymbol{I}_s$	No
Surface deformation gradient tensor	$\boldsymbol{F}_s$	Right
Elastic part of surface deformation gradient tensor	$\boldsymbol{F}_{s,e}$	Right
Plastic part of surface deformation gradient tensor	$\boldsymbol{F}_{s,p}$	Both
Interfacial Finger tensor	$\boldsymbol{B}_s$	No
Elastic part of interfacial Finger tensor	$\boldsymbol{B}_{s,e}$	No
Interfacial left-stretch tensor	$\boldsymbol{V}_s$	No
Rotation tensor	$\boldsymbol{R}_s$	Right
Surface velocity gradient tensor	$\boldsymbol{L}_s$	Left
Plastic part of surface velocity gradient tensor	$\boldsymbol{L}_{s,p}$	No
Surface rate-of-deformation tensor	$\boldsymbol{D}_s$	No
Plastic part of surface rate-of-deformation tensor	$\boldsymbol{D}_{s,p}$	No
Plastic part of surface spin tensor	$\boldsymbol{\Omega}_{s,p}$	No
Interfacial conformation tensor	$\boldsymbol{c}_s$	No

Declaration of competing interest

The authors declare that they have no known competing financial interests or personal relationships that could have appeared to influence the work reported in this paper.

Acknowledgements

The authors thank the Dutch Department of Economic Affairs for financial support from the Toeslag voor Topconsortia voor Kennis en Innovatie (TKI's), Netherlands.

Appendix A. Table of interfacial tensors

See Table A.1.

Appendix B. Auxiliary calculations for derivations

B.1. Surface determinant in terms of interfacial stretch ratios

The spectral form of $\boldsymbol{B}_s$ is given by

$$\boldsymbol{B}_s = \lambda_i^2 \boldsymbol{e}_{s,i}\boldsymbol{e}_{s,i}, \tag{B.1}$$

with λ_i, $i = 1,2$, the principal interfacial strain ratios and $\boldsymbol{e}_{s,i}$, $i = 1,2$, are the principal interfacial strain directions in the current configuration, which are of unit length. Note that $\boldsymbol{B}_s$ additionally has a zero eigenvalue with an eigenvector perpendicular to the interface. The left-polar decomposition of $\boldsymbol{F}_s$ reads [21]

$$\boldsymbol{F}_s = \boldsymbol{V}_s \cdot \boldsymbol{R}_s = \lambda_i \boldsymbol{e}_{s,i}\boldsymbol{e}_{s,i,0}, \tag{B.2}$$

where (see Eq. (B.1))

$$\boldsymbol{V}_s = \sqrt{\boldsymbol{B}_s} = \lambda_i \boldsymbol{e}_{s,i}\boldsymbol{e}_{s,i} \tag{B.3}$$

is the interfacial left stretch tensor. The tensor $\boldsymbol{R}_s = \boldsymbol{V}_s^{-1} \cdot \boldsymbol{F}_s$, with $\boldsymbol{V}_s^{-1}$ the Moore–Penrose inverse [22,23] of $\boldsymbol{V}_s$, is a rotation tensor ($\det_s(\boldsymbol{R}_s) = 1$), and $\boldsymbol{e}_{s,i,0}$, $i = 1,2$, are the dyad of vectors corresponding to $\boldsymbol{e}_{s,i}$ but in the reference configuration. The tensor $\boldsymbol{R}_s$ can be expressed as (see Eqs. (B.2)–(B.3))

$$\boldsymbol{R}_s = \boldsymbol{e}_{s,i}\boldsymbol{e}_{s,i,0}, \tag{B.4}$$

from which it becomes clear that, similar to $\boldsymbol{F}_s$, the directions on its left- and right-hand side are tangential to the interface in the current and reference configuration, respectively. Using Eqs. (16) and (B.2)–(B.3) and $\det_s(\boldsymbol{A}_s \cdot \boldsymbol{B}_s) = \det_s(\boldsymbol{A}_s)\det_s(\boldsymbol{B}_s)$ for interfacial tensors [21], it can be shown that

$$J_s = \det_s(\boldsymbol{F}_s) = \det_s(\boldsymbol{V}_s \cdot \boldsymbol{R}_s) = \det_s(\boldsymbol{V}_s)\det_s(\boldsymbol{R}_s) = \det_s(\boldsymbol{V}_s) = \lambda_1\lambda_2. \tag{B.5}$$

B.2. Time derivative of the (dual) base vectors and (dual) metric matrices

The time derivative of the base vectors $\boldsymbol{g}_i$ is given by

$$\dot{\boldsymbol{g}}_i = \left(\frac{\partial \boldsymbol{x}}{\partial \xi_i}\right)^{\cdot} = \frac{\partial \boldsymbol{u}}{\partial \xi_i} = \frac{\partial \boldsymbol{u}}{\partial \xi_j}\boldsymbol{g}^j \cdot \boldsymbol{g}_i = (\nabla_s \boldsymbol{u})^{\mathrm{T}} \cdot \boldsymbol{g}_i = \boldsymbol{L}_s \cdot \boldsymbol{g}_i, \tag{B.6}$$

where we have used Eqs. (2), (3) and (12).

The time derivative of the metric matrix g^{ij} is expressed as

$$\begin{aligned}
\dot{g}^{ij} &= -g^{ik}\dot{g}_{km}g^{mj} \\
&= -g^{ik}(\dot{\boldsymbol{g}}_k \cdot \boldsymbol{g}_m + \boldsymbol{g}_k \cdot \dot{\boldsymbol{g}}_m)g^{mj} \\
&= -g^{ik}\big((\boldsymbol{L}_s \cdot \boldsymbol{g}_k) \cdot \boldsymbol{g}_m + \boldsymbol{g}_k \cdot (\boldsymbol{L}_s \cdot \boldsymbol{g}_m)\big)g^{mj} \\
&= -\boldsymbol{g}^i \cdot (\boldsymbol{L}_s + \boldsymbol{L}_s^{\mathrm{T}}) \cdot \boldsymbol{g}^j \\
&= -\boldsymbol{g}^i \cdot \boldsymbol{I}_s \cdot (\boldsymbol{L}_s + \boldsymbol{L}_s^{\mathrm{T}}) \cdot \boldsymbol{I}_s \cdot \boldsymbol{g}^j \\
&= -\boldsymbol{g}^i \cdot 2\boldsymbol{D}_s \cdot \boldsymbol{g}^j,
\end{aligned} \tag{B.7}$$

where we have substituted Eqs. (5), (6) and (B.6), applied the product rule for differentiation, and applied $\dot{M} = -M(M^{-1})^{\cdot}M$ for any matrix M of which the inverse exists, to the matrix g^{ij} (see Eq. (8)).

The time derivative of the dual base vectors $\boldsymbol{g}^i$ reads

$$\begin{aligned}
\dot{\boldsymbol{g}}^i &= (g^{ij}\boldsymbol{g}_j)^{\cdot} \\
&= \dot{g}^{ij}\boldsymbol{g}_j + g^{ij}\dot{\boldsymbol{g}}_j \\
&= -\boldsymbol{g}^i \cdot 2\boldsymbol{D}_s \cdot \boldsymbol{g}^j\boldsymbol{g}_j + g^{ij}\boldsymbol{L}_s \cdot \boldsymbol{g}_j \\
&= -\boldsymbol{g}^i \cdot 2\boldsymbol{D}_s \cdot \boldsymbol{I}_s + \boldsymbol{L}_s \cdot \boldsymbol{g}^i \\
&= (\boldsymbol{L}_s - 2\boldsymbol{D}_s) \cdot \boldsymbol{g}^i,
\end{aligned} \tag{B.8}$$

in which we have used the product rule for differentiation and have substituted Eqs. (5), (11), (B.6) and (B.7).

B.3. Time derivative of the surface unit tensor

The evolution of $\boldsymbol{I}_s$ is derived by differentiating the third expression for $\boldsymbol{I}_s$ in Eq. (11) with respect to time:

$$\begin{aligned}
\dot{\boldsymbol{I}}_s &= (g^{ij}\boldsymbol{g}_i\boldsymbol{g}_j)^{\cdot} \\
&= \dot{g}^{ij}\boldsymbol{g}_i\boldsymbol{g}_j + g^{ij}\dot{\boldsymbol{g}}_i\boldsymbol{g}_j + g^{ij}\boldsymbol{g}_i\dot{\boldsymbol{g}}_j \\
&= -(\boldsymbol{g}^i \cdot 2\boldsymbol{D}_s \cdot \boldsymbol{g}^j)\boldsymbol{g}_i\boldsymbol{g}_j + \boldsymbol{L}_s \cdot g^{ij}\boldsymbol{g}_i\boldsymbol{g}_j + g^{ij}\boldsymbol{g}_i\boldsymbol{g}_j \cdot \boldsymbol{L}_s^{\mathrm{T}} \\
&= -2\boldsymbol{D}_s + \boldsymbol{L}_s \cdot \boldsymbol{I}_s + \boldsymbol{I}_s \cdot \boldsymbol{L}_s^{\mathrm{T}} \\
&= -2\boldsymbol{D}_s + \boldsymbol{L}_s + \boldsymbol{L}_s^{\mathrm{T}},
\end{aligned} \tag{B.9}$$

where we have applied the product rule for differentiation and have substituted Eqs. (10), (11), (B.6) and Eq. (B.7).

B.4. Rate of relative interfacial surface area change

Using the chain rule for differentiation, the time rate of change of J_s, defined in Eq. (23), can be written as

$$\frac{\dot{J}_s}{J_s} = \frac{1}{J_s}\frac{\partial J_s}{\partial \boldsymbol{F}_s} : \dot{\boldsymbol{F}}_s^{\mathrm{T}} = \boldsymbol{F}_s^{-\mathrm{T}} : \dot{\boldsymbol{F}}_s^{\mathrm{T}} = \mathrm{tr}(\dot{\boldsymbol{F}}_s \cdot \boldsymbol{F}_s^{-1}) = \mathrm{tr}(\boldsymbol{L}_s) = \mathrm{tr}(\boldsymbol{D}_s), \tag{B.10}$$

by substituting $\partial J_s/\partial \boldsymbol{F}_s = J_s\boldsymbol{F}_s^{-\mathrm{T}}$ and Eq. (28). The identity $\partial J_s/\partial \boldsymbol{F}_s = J_s\boldsymbol{F}_s^{-\mathrm{T}}$ can be shown to hold by first taking the derivative of $J_s^2 = c/2\|\boldsymbol{g}_1 \times \boldsymbol{g}_2\|^2 = c/2\sum_i([\boldsymbol{g}_1 \times \boldsymbol{g}_2]_i)^2 = c/2\sum_i(\epsilon_{ikl}g_{1,k}g_{2,l})^2$, with $c =$

$2/\|\boldsymbol{g}_{1,0}\times\boldsymbol{g}_{2,0}\|^2$, as follows (see Eq. (15))

$$\begin{aligned}\frac{\partial J_s^2}{\partial F_{s,pq}} &= c[\boldsymbol{g}_1\times\boldsymbol{g}_2]_i\frac{\partial}{\partial F_{s,pq}}(\epsilon_{ikl}g_{1,k}g_{2,l})\\ &= c[\boldsymbol{g}_1\times\boldsymbol{g}_2]_i\epsilon_{ikl}(\delta_{kp}g_{1,0,q}g_{2,l}+g_{1,k}\delta_{pl}g_{2,0,q})\\ &= c[\boldsymbol{g}_1\times\boldsymbol{g}_2]_i(\epsilon_{ipl}g_{1,0,q}g_{2,l}+\epsilon_{ikp}g_{1,k}g_{2,0,q})\\ &= c[\boldsymbol{g}_1\times\boldsymbol{g}_2]_i\epsilon_{ipk}(g_{1,0,q}g_{2,k}-g_{1,k}g_{2,0,q}),\end{aligned} \tag{B.11}$$

with ϵ_{ijk} the Levi-Civita symbol. Then, multiplication of Eq. (B.11) by $F_{s,rq}$ gives (see Eq. (15))

$$\begin{aligned}\frac{\partial J_s^2}{\partial F_{s,pq}}F_{s,rq} &= c[\boldsymbol{g}_1\times\boldsymbol{g}_2]_i\epsilon_{ipk}(F_{s,rq}g_{1,0,q}g_{2,k}-g_{1,k}F_{s,rq}g_{2,0,q})\\ &= c[\boldsymbol{g}_1\times\boldsymbol{g}_2]_i\epsilon_{ipk}(g_{1,r}g_{2,k}-g_{1,k}g_{2,r})\\ &= c(-\left[[\boldsymbol{g}_1\times\boldsymbol{g}_2]\times\boldsymbol{g}_2\right]_p g_{1,r}+\left[[\boldsymbol{g}_1\times\boldsymbol{g}_2]\times\boldsymbol{g}_1\right]_p g_{2,r})\\ &= c([(\boldsymbol{g}_2\cdot\boldsymbol{g}_2)g_{1,p}-(\boldsymbol{g}_1\cdot\boldsymbol{g}_2)g_{2,p}]g_{1,r}+[(\boldsymbol{g}_1\cdot\boldsymbol{g}_1)g_{2,p}\\ &\quad-(\boldsymbol{g}_1\cdot\boldsymbol{g}_2)g_{1,p}]g_{2,r}),\end{aligned} \tag{B.12}$$

where the vector triple product is related to the inner product using $(\boldsymbol{a}\times\boldsymbol{b})\times\boldsymbol{c}=\boldsymbol{b}(\boldsymbol{a}\cdot\boldsymbol{c})-\boldsymbol{a}(\boldsymbol{b}\cdot\boldsymbol{c})$. In tensor notation, Eq. (B.12) is rewritten as

$$\boldsymbol{A}_s\equiv\frac{\partial J_s^2}{\partial\boldsymbol{F}_s}\cdot\boldsymbol{F}_s^{\mathrm{T}}=c([(\boldsymbol{g}_2\cdot\boldsymbol{g}_2)\boldsymbol{g}_1-(\boldsymbol{g}_1\cdot\boldsymbol{g}_2)\boldsymbol{g}_2]\boldsymbol{g}_1+[(\boldsymbol{g}_1\cdot\boldsymbol{g}_1)\boldsymbol{g}_2-(\boldsymbol{g}_1\cdot\boldsymbol{g}_2)\boldsymbol{g}_1]\boldsymbol{g}_2). \tag{B.13}$$

To show that $\boldsymbol{A}_s$ is proportional to $\boldsymbol{I}_s$, we compute (see Eq. (3))

$$\begin{aligned}\boldsymbol{A}_s\cdot\boldsymbol{g}^1 &= c[(\boldsymbol{g}_2\cdot\boldsymbol{g}_2)\boldsymbol{g}_1-(\boldsymbol{g}_1\cdot\boldsymbol{g}_2)\boldsymbol{g}_2]\\ &= c[(\boldsymbol{g}_2\cdot\boldsymbol{g}_2)\boldsymbol{g}_1-(\boldsymbol{g}_1\cdot\boldsymbol{g}_2)\boldsymbol{g}_2]\cdot\boldsymbol{g}_k\boldsymbol{g}^k\\ &= c[(\boldsymbol{g}_2\cdot\boldsymbol{g}_2)(\boldsymbol{g}_1\cdot\boldsymbol{g}_1)-(\boldsymbol{g}_1\cdot\boldsymbol{g}_2)^2]\cdot\boldsymbol{g}^1\\ &= a\boldsymbol{g}^1,\end{aligned} \tag{B.14}$$

with $a=c[(\boldsymbol{g}_2\cdot\boldsymbol{g}_2)(\boldsymbol{g}_1\cdot\boldsymbol{g}_1)-(\boldsymbol{g}_1\cdot\boldsymbol{g}_2)^2]$. Similarly, it can be shown that $\boldsymbol{A}_s\cdot\boldsymbol{g}^2=a\boldsymbol{g}^2$. So $\boldsymbol{A}_s=a\boldsymbol{I}_s$, since $\boldsymbol{A}_s$ is tangential to the interface and it maps any tangential vector by keeping its direction. Tensor $\boldsymbol{A}_s$ can be rewritten using the chain rule for differentiation as (see Eq. (B.13))

$$\boldsymbol{A}_s=2J_s\frac{\partial J_s}{\partial\boldsymbol{F}_s}\cdot\boldsymbol{F}_s^{\mathrm{T}}, \tag{B.15}$$

from which it can be concluded that

$$\frac{\partial J_s}{\partial\boldsymbol{F}_s}=\frac{a}{2J_s}\boldsymbol{F}_s^{-\mathrm{T}}=J_s\boldsymbol{F}_s^{-\mathrm{T}}, \tag{B.16}$$

since (see Eq. (16))

$$\begin{aligned}a &= c[(\boldsymbol{g}_2\cdot\boldsymbol{g}_2)(\boldsymbol{g}_1\cdot\boldsymbol{g}_1)-(\boldsymbol{g}_1\cdot\boldsymbol{g}_2)^2]\\ &= c\|\boldsymbol{g}_1\times\boldsymbol{g}_2\|^2\\ &= 2\|\boldsymbol{g}_{1,0}\times\boldsymbol{g}_{2,0}\|^{-2}\|\boldsymbol{g}_1\times\boldsymbol{g}_2\|^2\\ &= 2J_s^2.\end{aligned} \tag{B.17}$$

B.5. Evolution equation for the elastic part of the deformation

The split of the surface deformation gradient tensor $\boldsymbol{F}_s$ into an elastic part $\boldsymbol{F}_{s,e}$ and a plastic part $\boldsymbol{F}_{s,p}$ reads (see Eq. (25))

$$\boldsymbol{F}_s=\boldsymbol{F}_{s,e}\cdot\boldsymbol{F}_{s,p}. \tag{B.18}$$

The tensors $\boldsymbol{F}_{s,e}$ and $\boldsymbol{F}_{s,p}$ are functions of the curvilinear coordinates ξ and time t, just as $\boldsymbol{F}_s$ (see Eqs. (2)–(3) and (15)). These tensors and their inverses operate in the following way:

$$\begin{aligned}d\boldsymbol{x}=\boldsymbol{F}_{s,e}\cdot d\boldsymbol{x}_I,\quad d\boldsymbol{x}_I=\boldsymbol{F}_{s,p}\cdot d\boldsymbol{x}_0,\\ d\boldsymbol{x}_I=\boldsymbol{F}_{s,e}^{-1}\cdot d\boldsymbol{x},\quad d\boldsymbol{x}_0=\boldsymbol{F}_{s,p}^{-1}\cdot d\boldsymbol{x}_I,\end{aligned} \tag{B.19}$$

where $d\boldsymbol{x}_0$, $d\boldsymbol{x}_I$ and $d\boldsymbol{x}$ are infinitesimal interface line elements in the reference, intermediate and current configurations, respectively, see Fig. 2. Eq. (B.19) shows that $\boldsymbol{F}_{s,p}$ maps infinitesimal interface line elements from the reference configuration onto the intermediate configuration, which in their turn are mapped by $\boldsymbol{F}_{s,e}$ onto the current configuration, point by point (constant ξ). Since the mapping is linear, and the reference and current configurations are in each point ξ described by just two linearly independent vectors in 3D space, the intermediate configuration can also in each point be described by a plane in 3D space. However, note that the intermediate configuration is not a tangent space, since it is not obtained by differentiation of a parametrised curved surface. Still, we can introduce the base vectors $\boldsymbol{g}_{i,I}$ and dual base vectors $\boldsymbol{g}_I^i$ for each point on the interface in the intermediate configuration. This allows us to express the elastic and plastic parts of the deformation in a similar manner as $\boldsymbol{F}_s$ (see Eqs. (15) and (17)):

$$\begin{aligned}\boldsymbol{F}_{s,e}=\boldsymbol{g}_i\boldsymbol{g}_I^i,\quad \boldsymbol{F}_{s,p}=\boldsymbol{g}_{i,I}\boldsymbol{g}_0^i,\\ \boldsymbol{F}_{s,e}^{-1}=\boldsymbol{g}_{i,I}\boldsymbol{g}^i,\quad \boldsymbol{F}_{s,p}^{-1}=\boldsymbol{g}_{i,0}\boldsymbol{g}_I^i.\end{aligned} \tag{B.20}$$

This is convenient for deriving the evolution equation for $\boldsymbol{F}_{s,e}$ as presented in Eq. (42). For example, the surface unit tensor in the intermediate configuration $\boldsymbol{I}_{s,I}$ can now be expressed as (see also Eqs. (18)–(19))

$$\boldsymbol{I}_{s,I}=\boldsymbol{F}_{s,e}^{-1}\cdot\boldsymbol{F}_{s,e}=\boldsymbol{F}_{s,p}\cdot\boldsymbol{F}_{s,p}^{-1}. \tag{B.21}$$

Taking the time derivative of Eq. (B.18) at constant curvilinear coordinates ξ (see Eq. (29)) using the product rule for differentiation, yields

$$\dot{\boldsymbol{F}}_s=\dot{\boldsymbol{F}}_{s,e}\cdot\boldsymbol{F}_{s,p}+\boldsymbol{F}_{s,e}\cdot\dot{\boldsymbol{F}}_{s,p}. \tag{B.22}$$

Multiplying Eq. (B.22) by $\boldsymbol{F}_{s,p}^{-1}$ from the right, substituting Eqs. (28), (B.18) and (B.21), using that $\boldsymbol{F}_{s,e}\cdot\boldsymbol{I}_{s,I}=\boldsymbol{F}_{s,e}$ and $\boldsymbol{F}_{s,p}^{-1}\cdot\boldsymbol{I}_{s,I}=\boldsymbol{F}_{s,p}^{-1}$ (see Eq. (B.20)), and rearranging terms, gives

$$\dot{\boldsymbol{F}}_{s,e}\cdot\boldsymbol{I}_{s,I}=(\boldsymbol{L}_s-\boldsymbol{L}_{s,p})\cdot\boldsymbol{F}_{s,e}, \tag{B.23}$$

where we have defined the plastic surface velocity gradient tensor in the current configuration $\boldsymbol{L}_{s,p}=\boldsymbol{F}_{s,e}\cdot\dot{\boldsymbol{F}}_{s,p}\cdot\boldsymbol{F}_{s,p}^{-1}\cdot\boldsymbol{F}_{s,e}^{-1}$.

B.6. Thermodynamic consistency

In this appendix, we examine the implications of nonequilibrium thermodynamics arguments on the constitutive relations for the interfacial stress tensor $\boldsymbol{\tau}_s$ and for the plastic surface rate-of-deformation tensor $\boldsymbol{D}_{s,p}$. To that end, we proceed along the procedure outlined in [38] – as explained in the following – , but applied here to an interface. It is pointed out that the following steps are taken in order to check the thermodynamic admissibility of interfacial constitutive relations, and the interest is not in solving a concrete dynamic problem in which the interface is coupled to the adjacent bulk; so doing gives us the freedom to neglect the coupling to the adjacent bulk phases. This implies that the interface can be considered as a closed system, in both a thermal and mechanical sense.

We depart from specifying expressions for the total energy and entropy of the interface. Namely, these quantities are written as integrals over the corresponding densities. For the further procedure, it is beneficial to express the integrals in the reference state, since in that case the interfacial domain does not change in the course of time. In particular, we write

$$E_s=\int\left(\rho_{s,0}\frac{u^2}{2}+\hat{e}_s\left(J_s,T_s,\tilde{c}_s\right)\right)dA_0, \tag{B.24}$$

$$S_s=\int\hat{s}_s\left(J_s,T_s,\tilde{c}_s\right)dA_0, \tag{B.25}$$

where $\rho_{s,0}$ is the interfacial mass density in the reference configuration, $\hat{e}_s$ and $\hat{s}_s$ denote the densities of internal energy and entropy per unit area in the reference configuration, T_s is the interfacial temperature, and $\tilde{c}_s$ is the internal interfacial deformation variable, which will be specified later.

Before proceeding with the application of the thermodynamics conditions on the constitutive equations in the model, let us first examine the time evolution of the energy. Using that the integration domain in the reference state does not change in time, and by virtue of the chain rule of differential calculus, one obtains

$$\dot{E}_\mathrm{s} = \int \left(\rho_{\mathrm{s},0} \boldsymbol{u} \cdot \dot{\boldsymbol{u}} + \frac{\partial \hat{e}_\mathrm{s}}{\partial J_\mathrm{s}} \dot{J}_\mathrm{s} + \frac{\partial \hat{e}_\mathrm{s}}{\partial T_\mathrm{s}} \dot{T}_\mathrm{s} + \frac{\partial \hat{e}_\mathrm{s}}{\partial \tilde{\boldsymbol{c}}_\mathrm{s}} : \dot{\tilde{\boldsymbol{c}}}_\mathrm{s} \right) dA_0 \,. \tag{B.26}$$

To proceed, we first examine particularly the first term on the r.h.s. of Eq. (B.26). For a single component interface without adjacent bulk phases (see comment above) and in the absence of body forces, the momentum balance is given by $\rho_\mathrm{s} \dot{\boldsymbol{u}} = \nabla_\mathrm{s} \cdot \boldsymbol{\tau}_\mathrm{s}$ [21], where the latter can be expressed in the form $\rho_{\mathrm{s},0} \dot{\boldsymbol{u}} = \nabla_{\mathrm{s},0} \cdot \left(J_\mathrm{s} \boldsymbol{F}_\mathrm{s}^{-1} \cdot \boldsymbol{\tau}_\mathrm{s} \right)$. With this, one obtains

$$\begin{aligned} \int \rho_{\mathrm{s},0} \boldsymbol{u} \cdot \dot{\boldsymbol{u}} dA_0 &= \int \boldsymbol{u} \cdot \left(\nabla_{\mathrm{s},0} \cdot \left(J_\mathrm{s} \boldsymbol{F}_\mathrm{s}^{-1} \cdot \boldsymbol{\tau}_\mathrm{s} \right) \right) dA_0 \\ &= \int \left(\nabla_{\mathrm{s},0} \cdot \boldsymbol{n}_0 \right) \left(\boldsymbol{n}_0 \cdot \boldsymbol{F}_\mathrm{s}^{-1} \cdot \boldsymbol{\tau}_\mathrm{s} \cdot \boldsymbol{u} \right) J_\mathrm{s} dA_0 \\ &\quad - \int \left(\nabla_\mathrm{s} \boldsymbol{u} \right) : \boldsymbol{\tau}_\mathrm{s} J_\mathrm{s} dA_0 \,, \end{aligned} \tag{B.27}$$

where $\boldsymbol{n}_0$ is the unit-normal vector on the interface in the reference configuration. In the second equality, we have used the surface divergence theorem [42] as well as Eq. (20); boundary terms are absent if the integration domain is closed or under particular conditions on symmetry. The first term on the right-hand side of Eq. (B.27) vanishes since $\boldsymbol{n}_0$ is perpendicular to $\boldsymbol{F}_\mathrm{s}^{-1}$ (see Eq. (17)). Inserting Eq. (B.27) into Eq. (B.26), and using $\dot{J}_\mathrm{s} = J_\mathrm{s} (\nabla_\mathrm{s} \cdot \boldsymbol{u})$ (see Eq. (31)), one finds

$$\dot{E}_\mathrm{s} = \int \left(-J_\mathrm{s} \boldsymbol{\tau}_\mathrm{s} : \left(\nabla_\mathrm{s} \boldsymbol{u} \right) + J_\mathrm{s} \frac{\partial \hat{e}_\mathrm{s}}{\partial J_\mathrm{s}} (\nabla_\mathrm{s} \cdot \boldsymbol{u}) + \frac{\partial \hat{e}_\mathrm{s}}{\partial T_\mathrm{s}} \dot{T}_\mathrm{s} + \frac{\partial \hat{e}_\mathrm{s}}{\partial \tilde{\boldsymbol{c}}_\mathrm{s}} : \dot{\tilde{\boldsymbol{c}}}_\mathrm{s} \right) dA_0 \,. \tag{B.28}$$

With this auxiliary calculation, we have paved the way for implementing the thermodynamic conditions in the elastoviscoplastic interface constitutive model.

In the course of *reversible* (i.e. non-dissipative) dynamics, both the total energy as well as the entropy are conserved, i.e., $dE_\mathrm{s}/dt|_\mathrm{rev} = 0$ and $dS_\mathrm{s}/dt|_\mathrm{rev} = 0$ [29,38]. Using Eq. (B.28) and an analogous calculation for the entropy, these two conditions can be cast into the following local conditions,

$$-J_\mathrm{s} \boldsymbol{\tau}_\mathrm{s} : \left(\nabla_\mathrm{s} \boldsymbol{u} \right) + J_\mathrm{s} \frac{\partial \hat{e}_\mathrm{s}}{\partial J_\mathrm{s}} (\nabla_\mathrm{s} \cdot \boldsymbol{u}) + \frac{\partial \hat{e}_\mathrm{s}}{\partial T_\mathrm{s}} \dot{T}_\mathrm{s}|_\mathrm{rev} + \frac{\partial \hat{e}_\mathrm{s}}{\partial \tilde{\boldsymbol{c}}_\mathrm{s}} : \dot{\tilde{\boldsymbol{c}}}_\mathrm{s}|_\mathrm{rev} = 0 \,, \tag{B.29}$$

$$J_\mathrm{s} \frac{\partial \hat{s}_\mathrm{s}}{\partial J_\mathrm{s}} (\nabla_\mathrm{s} \cdot \boldsymbol{u}) + \frac{\partial \hat{s}_\mathrm{s}}{\partial T_\mathrm{s}} \dot{T}_\mathrm{s}|_\mathrm{rev} + \frac{\partial \hat{s}_\mathrm{s}}{\partial \tilde{\boldsymbol{c}}_\mathrm{s}} : \dot{\tilde{\boldsymbol{c}}}_\mathrm{s}|_\mathrm{rev} = 0 \,. \tag{B.30}$$

Eq. (B.30) can be solved for $\dot{T}_\mathrm{s}|_\mathrm{rev}$, which in turn is then inserted into Eq. (B.29), from which the interfacial stress tensor can be determined for given reversible dynamics of $\tilde{\boldsymbol{c}}_\mathrm{s}$. Particularly, performing these calculations for upper-convected behaviour (Eqs. (46)–(47)) and lower-convected behaviour (Eqs. (49)–(50)) of $\tilde{\boldsymbol{c}}_\mathrm{s}$, respectively, one obtains,

$$\boldsymbol{\tau}_\mathrm{s} = \frac{\partial \hat{\psi}_\mathrm{s}}{\partial J_\mathrm{s}} \boldsymbol{I}_\mathrm{s} \pm \frac{2}{J_\mathrm{s}} \tilde{\boldsymbol{c}}_\mathrm{s} \cdot \frac{\partial \hat{\psi}_\mathrm{s}}{\partial \tilde{\boldsymbol{c}}_\mathrm{s}} \,, \tag{B.31}$$

where the "+" is to be used if $\tilde{\boldsymbol{c}}_\mathrm{s} = \boldsymbol{B}_{\mathrm{s,e}}$ is upper-convected, and "−" is to be used if $\tilde{\boldsymbol{c}}_\mathrm{s} = \boldsymbol{B}_{\mathrm{s,e}}^{-1}$ is lower-convected; $\hat{\psi}_\mathrm{s} = \hat{e}_\mathrm{s} - T_\mathrm{s} \hat{s}_\mathrm{s}$ denotes the interfacial Helmholtz free energy density per unit area in the reference configuration.

In the course of *irreversible* (i.e., dissipative) dynamics, the total energy is conserved, i.e., $dE/dt|_\mathrm{irr} = 0$, while the entropy must not decrease, i.e., $dS/dt|_\mathrm{irr} \geq 0$. Also in this case, we employ the chain rule in order to relate these conditions to the time evolution of the quantities of interest. In the absence of irreversible contributions to the momentum balance, i.e., in the absence of viscous stresses, one can rewrite $dE/dt|_\mathrm{irr} = 0$ and $dS/dt|_\mathrm{irr} \geq 0$ into the following local conditions,

$$\frac{\partial \hat{e}_\mathrm{s}}{\partial T_\mathrm{s}} \dot{T}_\mathrm{s}|_\mathrm{irr} + \frac{\partial \hat{e}_\mathrm{s}}{\partial \tilde{\boldsymbol{c}}_\mathrm{s}} : \dot{\tilde{\boldsymbol{c}}}_\mathrm{s}|_\mathrm{irr} = 0 \,, \tag{B.32}$$

$$\frac{\partial \hat{s}_\mathrm{s}}{\partial T_\mathrm{s}} \dot{T}_\mathrm{s}|_\mathrm{irr} + \frac{\partial \hat{s}_\mathrm{s}}{\partial \tilde{\boldsymbol{c}}_\mathrm{s}} : \dot{\tilde{\boldsymbol{c}}}_\mathrm{s}|_\mathrm{irr} \geq 0 \,. \tag{B.33}$$

Eq. (B.32) can be solved for $\dot{T}_\mathrm{s}|_\mathrm{irr}$, which in turn is then inserted into Eq. (B.33), from which one obtains a condition on the plastic surface rate-of-deformation tensor. Particularly, performing these calculations for the irreversible dynamics of $\tilde{\boldsymbol{c}}_\mathrm{s} = \boldsymbol{B}_{\mathrm{s,e}}$ with upper-convected behaviour (Eqs. (46)–(47)) and of $\tilde{\boldsymbol{c}}_\mathrm{s} = \boldsymbol{B}_{\mathrm{s,e}}^{-1}$ with lower-convected behaviour (Eqs. (49)–(50)), respectively, one obtains,

$$\boldsymbol{\tau}_{\mathrm{s,c}} : \boldsymbol{D}_{\mathrm{s,p}} \geq 0 \,, \tag{B.34}$$

for both cases, where $\boldsymbol{\tau}_{\mathrm{s,c}}$ denotes the second, conformation-dependent contribution to the stress tensor on the right-hand side of Eq. (B.31).

References

[1] V. Sharma, A. Jaishankar, Y.-C. Wang, G. McKinley, Rheology of globular proteins: apparent yield stress, high shear rate viscosity and interfacial viscoelasticity of bovine serum albumin solutions, Soft Matter 7 (11) (2011) 5150–5160, http://dx.doi.org/10.1039/C0SM01312A.

[2] D. Zang, E. Rio, G. Delon, D. Langevin, B. Wei, B. Binks, Influence of the contact angle of silica nanoparticles at the air–water interface on the mechanical properties of the layers composed of these particles, Mol. Phys. 109 (7–10) (2011) 1057–1066, http://dx.doi.org/10.1080/00268976.2010.542778.

[3] J.-M. Jung, D. Gunes, R. Mezzenga, Interfacial activity and interfacial shear rheology of native β-lactoglobulin monomers and their heat-induced fibers, Langmuir 26 (19) (2010) 15366–15375, http://dx.doi.org/10.1021/la102721m.

[4] A. Martin, M. Bos, M. Cohen Stuart, T. van Vliet, Stress-strain curves of adsorbed protein layers at the air/water interface measured with surface shear rheology, Langmuir 18 (4) (2002) 1238–1243, http://dx.doi.org/10.1021/la011176x.

[5] K. Moran, A. Yeung, J. Masliyah, The viscoplastic properties of crude oil–water interfaces, Chem. Eng. Sci. 61 (18) (2006) 6016–6028, http://dx.doi.org/10.1016/j.ces.2006.05.026.

[6] H. Hilles, F. Monroy, L. Bonales, F. Ortega, R. Rubio, Fourier-Transform rheology of polymer Langmuir monolayers: Analysis of the non-linear and plastic behaviors, Adv. Colloid Interface Sci. 122 (1) (2006) 67–77, http://dx.doi.org/10.1016/j.cis.2006.06.013.

[7] J. Ferri, C. Kotsmar, R. Miller, From surfactant adsorption kinetics to asymmetric nanomembrane mechanics: Pendant drop experiments with subphase exchange, Adv. Colloid Interface Sci. 161 (1) (2010) 29–47, http://dx.doi.org/10.1016/j.cis.2010.08.002.

[8] K. Masschaele, J. Fransaer, J. Vermant, Flow-induced structure in colloidal gels: direct visualization of model 2D suspensions, Soft Matter 7 (17) (2011) 7717–7726, http://dx.doi.org/10.1039/c1sm05271c.

[9] I. Buttinoni, Z. Zell, T. Squires, L. Isa, Colloidal binary mixtures at fluid-fluid interfaces under steady shear: structural, dynamical and mechanical response, Soft Matter 11 (42) (2015) 8313–8321, http://dx.doi.org/10.1039/c5sm01693b.

[10] A. Alicke, S. Simon, J. Sjöblom, J. Vermant, Assessing the interfacial activity of insoluble asphaltene layers: Interfacial rheology versus interfacial tension, Langmuir 36 (49) (2020) 14942–14959, http://dx.doi.org/10.1021/acs.langmuir.0c02234.

[11] N. Jaensson, P. Anderson, J. Vermant, Computational interfacial rheology, J. Non-Newton. Fluid Mech. 290 (2021) 104507, http://dx.doi.org/10.1016/j.jnnfm.2021.104507.

[12] D. Edwards, H. Brenner, D. Wasan, Interfacial Transport Processes and Rheology, Butterworth-Heinemann, 1991, http://dx.doi.org/10.1016/C2009-0-26916-9.

[13] M. Hütter, T. Tervoort, Thermodynamic considerations on non-isothermal finite anisotropic elasto-viscoplasticity, J. Non-Newton. Fluid Mech. 152 (1) (2008) 53–65, http://dx.doi.org/10.1016/j.jnnfm.2007.10.008.

[14] M. Pepicelli, T. Verwijlen, T. Tervoort, J. Vermant, Characterization and modelling of Langmuir interfaces with finite elasticity, Soft Matter 13 (35) (2017) 5977–5990, http://dx.doi.org/10.1039/C7SM01100H.

[15] L. Sagis, Dynamic properties of interfaces in soft matter: Experiments and theory, Rev. Modern Phys. 83 (4) (2011) 1367–1403, http://dx.doi.org/10.1103/RevModPhys.83.1367.

[16] C. Balemans, M. Hulsen, P. Anderson, Modeling of complex interfaces for pendant drop experiments, Rheol. Acta 55 (10) (2016) 801–822, http://dx.doi.org/10.1007/s00397-016-0956-1.

[17] J. Gounley, G. Boedec, M. Jaeger, M. Leonetti, Influence of surface viscosity on droplets in shear flow, J. Fluid Mech. 791 (2016) 464–494, http://dx.doi.org/10.1017/jfm.2016.39.

[18] M. Carrozza, M. Hulsen, P. Anderson, Benchmark solutions for flows with rheologically complex interfaces, J. Non-Newton. Fluid Mech. 286 (2020) 104436, http://dx.doi.org/10.1016/j.jnnfm.2020.104436.

[19] S. Ozan, H. Jakobsen, Effect of surface viscoelasticity on the film drainage and the interfacial mobility, Int. J. Multiph. Flow. 130 (2020) 103377, http://dx.doi.org/10.1016/j.ijmultiphaseflow.2020.103377.

[20] E. de Kinkelder, L. Sagis, S. Aland, A numerical method for the simulation of viscoelastic fluid surfaces, J. Comput. Phys. 440 (2021) 110413, http://dx.doi.org/10.1016/j.jcp.2021.110413.
[21] J. Slattery, L. Sagis, E. Oh, Interfacial Transport Phenomena, Springer, 2007, http://dx.doi.org/10.1007/978-0-387-38442-9.
[22] E. Moore, On the reciprocal of the general algebraic matrix, Bull. Amer. Math. Soc. 26 (9) (1920) 394–395, http://dx.doi.org/10.1090/S0002-9904-1920-03322-7.
[23] R. Penrose, A generalized inverse for matrices, Math. Proc. Camb. Phil. Soc. 51 (3) (1955) 406–413, http://dx.doi.org/10.1017/S0305004100030401.
[24] E. Lee, Elastic-plastic deformation at finite strains, J. Appl. Mech. 36 (1) (1969) 1–6, http://dx.doi.org/10.1115/1.3564580.
[25] M. Boyce, D. Parks, A. Argon, Large inelastic deformation of glassy polymers. part I: rate dependent constitutive model, Mech. Mater. 7 (1) (1988) 15–33, http://dx.doi.org/10.1016/0167-6636(88)90003-8.
[26] R. Bird, R. Armstrong, O. Hassager, Dynamics of Polymeric Liquids, Volume 1: Fluid Mechanics, second ed., John Wiley & Sons Inc, 1987.
[27] R. Gordon, W. Schowalter, Anisotropic fluid theory: A different approach to the dumbbell theory of dilute polymer solutions, Trans. Soc. Rheol. 16 (1) (1972) 79–97, http://dx.doi.org/10.1122/1.549256.
[28] P. Wapperom, M. Hulsen, Thermodynamics of viscoelastic fluids: The temperature equation, J. Rheol. 42 (5) (1998) 999–1019, http://dx.doi.org/10.1122/1.550922.
[29] H. Öttinger, Beyond Equilibrium Thermodynamics, John Wiley & Sons Inc, 2005, http://dx.doi.org/10.1002/0471727903.
[30] T. Tervoort, R. Smit, W. Brekelmans, L. Govaert, A constitutive equation for the elasto-viscoplastic deformation of glassy polymers, Mech. Time-Dependent Mater. 1 (3) (1997) 269–291, http://dx.doi.org/10.1023/A:1009720708029.
[31] L. Govaert, P. Timmermans, W. Brekelmans, The influence of intrinsic strain softening on strain localization in polycarbonate: Modeling and experimental validation, J. Eng. Mater. Technol. 122 (2) (1999) 177–185, http://dx.doi.org/10.1115/1.482784.
[32] E. Klompen, T. Engels, L. Govaert, H. Meijer, Modeling of the postyield response of glassy polymers: Influence of thermomechanical history, Macromolecules 38 (16) (2005) 6997–7008, http://dx.doi.org/10.1021/ma050498v.
[33] L. van Breemen, E. Klompen, L. Govaert, H. Meijer, Extending the EGP constitutive model for polymer glasses to multiple relaxation times, J. Mech. Phys. Solids 59 (10) (2011) 2191–2207, http://dx.doi.org/10.1016/j.jmps.2011.05.001.
[34] T. Tervoort, E. Klompen, L. Govaert, A multi-mode approach to finite, three-dimensional, nonlinear viscoelastic behavior of polymer glasses, J. Rheol. 40 (5) (1996) 779–797, http://dx.doi.org/10.1122/1.550755.
[35] M. Hütter, T. Tervoort, Finite anisotropic elasticity and material frame indifference from a nonequilibrium thermodynamics perspective, J. Non-Newton. Fluid Mech. 152 (1) (2008) 45–52, http://dx.doi.org/10.1016/j.jnnfm.2007.10.009.
[36] M. Hütter, C. Luap, H. Öttinger, Energy elastic effects and the concept of temperature in flowing polymeric liquids, Rheol. Acta 48 (3) (2009) 301–316, http://dx.doi.org/10.1007/s00397-008-0318-8.
[37] C. Truesdell, W. Noll, the Non-Linear Field Theories of Mechanics, Springer-Verlag Berlin Heidelberg, 2004, http://dx.doi.org/10.1007/978-3-662-10388-3.
[38] M. Hütter, L. van Breemen, Microstructural model for the plasticity of amorphous solids, J. Appl. Polym. Sci. 125 (6) (2012) 4376–4389, http://dx.doi.org/10.1002/app.36576.
[39] F. Morrison, Understanding Rheology, Oxford University Press, 2001.
[40] J. Snoeijer, A. Pandey, M. Herrada, J. Eggers, The relationship between viscoelasticity and elasticity, Proc. R. Soc. A 476 (2243) (2020) 20200419, http://dx.doi.org/10.1098/rspa.2020.0419.
[41] E. Süli, D. Mayers, An Introduction to Numerical Analysis, Cambridge University Press, 2003, http://dx.doi.org/10.1017/CBO9780511801181.
[42] C. Weatherburn, Differential Geometry of Three Dimensions, Cambridge University Press, 1955.